# POLITECNICO DI TORINO

Master of Science Degree in Automotive Engineering

Master Thesis

# Finite Element modelling of Moving Progressive Deformable Barrier


*Academic Supervisor*

Prof. Alessandro SCATTINA

*Company Supervisor*

Ing. Erik BALDOIN

*Candidate*

Fabio TONDO


FIAT CHRYSLER AUTOMOBILES

CRF CENTRO RICERCHE FIAT

A.A. 2019/2020

## Abstract

This work concerns the creation of a finite element model of the moving progressive deformable barrier, built with solid elements, that includes an advanced failure criterion able to model the bottoming of the barrier and that provides a reasonable simulation time when compared to a reference barrier model. The honeycomb material law is characterized through numerical tests on scaled models of the barrier block and finally, the virtual MPDB crash test is carried out, impacting the barrier against a modern vehicle.

# Table of Contents

# 1. Introduction

This thesis contains the work done during the internship period in Centro Ricerche Fiat, aimed at the creation of an optimized finite element model of a frontal crash barrier, the Progressive Deformable Barrier, introduced in 2020 by Euro NCAP in its testing.

The barrier virtual model has been built using the solver LS-Dyna and has been designed from the ground up, choosing state of the art solutions like hexahedral elements, honeycomb material and cohesive elements. The honeycomb material has been characterized with a scaled model from the front block performing various tests in order to find numerically the values for the material parameters. Afterwards, the full-scale front block is considered and then the full barrier, where a fine-tuning of the parameters is done to ensure that the model works as expected. Finally, a virtual crash test with a vehicle provided by FCA is performed to evaluate the difference between the barrier designed and a reference one.

The thesis is organized so that in the first three chapters the characteristics of crash tests, of crash barrier and of honeycomb materials are explained. In the successive two chapters the virtual reference model for this barrier is investigated and the possible alternatives are considered, examining the logic behind the cards involved. The next three chapters are about the actual model creation, the problems encountered and the solution found to overcome them, while the successive chapter is a summary of all the cards used, useful to replicate this work if needed.

As it will be explained at the end of this thesis, satisfactory results have been obtained from this model mainly thanks to the failure criteria adopted, pushing to the limit the capabilities of one constraint card in the solver code.

## 2. Euro NCAP

Euro NCAP (European New Car Assessment Programme) is a voluntary association with the aim of evaluating the safety of vehicles on market in order to promote safer cars for consumers. From a legal stand point Car Manufacturers must respect a stringent set of rules imposed by government bodies like European Union. A significant subset of rules regards structural safety during a crash and takes the name of homologation test. Euro NCAP believes that such tests are not enough to ensure the thorough safety of passenger and decided to put new vehicles under more stringent test and evaluating them via a 0 to 5 stars rating. A 0 stars rating means that the car is compliant with homologation test but lacks modern safety technology, while a 5 stars rating represent a very safe vehicle with all the modern technologies to prevent and reduce the crash occurrences and consequences.

The rating is based on geometric measurements of the passenger compartment after the impact and on the data logged from high-tech dummies that are able to record different types of external solicitations perceived by the different body segments of the human body. There is a great variety of manikins that differ for technical specifications (front and side dummies) and for height and weight (adults and kids of different age), but all the dummies are capable to provide reliable biomechanical data, used to assign a score based on the injury criteria.

The criteria are studied considering the physiology of the different body parts, so for example the head criterion is based on deceleration and also on the exposure time of the latter. Neck criterion's thresholds are different if in flexion or extension, while also shear strain is taken in consideration. Chest criterion is created considering both crushing and viscous injuries, that means designing a threshold on maximum compression and maximum compression rate.

For the lower limbs the criteria are easier, because the different portions are approximated to rods and so threshold on maximum load and maximum displacement are imposed.

Over time more attention has been put into preventing accidents from happening and protecting vulnerable road users like pedestrians and cyclists, so the final rating is a

properly weighted average of all these tests results.


*Figure 1 Euro NCAP evaluation system*

Since its foundation in 1996, the association's biggest achievement has been driving consumer focus and car manufacturer resources into crashworthiness of brand-new passenger cars.

Indeed, during the years, we saw the introduction in the market of innovative solutions to improve the structural energy absorption, the structural stability, the passengers' restraint systems, such as more advanced airbags and safety belts with pretensioners and load limiters, and new electronic systems to reduce the occurrence of a crash.

Nowadays Euro NCAP performs a large variety of tests to evaluate the passive safety of a vehicle, like Mobile Progressive Deformable Barrier test, Full Width Rigid Barrier test, Mobile Side Impact Barrier test, Side pole test, Far Side Impact test. Other assessment regards Whiplash test (performed only on a seat and not on the entire vehicle) and the ease with which passengers can get rescued and extricated from the vehicle after a crash.

The **mobile progressive deformable barrier test**, introduced in 2020, is a frontal impact test against the MPDB barrier with 50% overlap where either the vehicle and the 1400 kg carriage on which the barrier in mounted on travel at 50 km/h in opposite directions. The test replicates a crash between the test vehicle and a typical mid-size family

car. Two frontal impact dummies representing a defined adult male percentile are seated in the front and child dummies are placed in child restraints in the rear seats. The dummies, vehicle and trolley are instrumented to record the forces and decelerations to which the occupants would be subjected. Several aspects of a car's safety are assessed in this test. To protect the test car's occupants, crash forces have to be efficiently directed to parts of the car where the energy can be efficiently and safely absorbed. The front crumple zone must collapse in a controlled way, leaving the passenger compartment as undeformed as possible while, at the same time, not exposing the occupants to dangerously high levels of deceleration. Rearward movement of the steering wheel and the pedals must be limited if serious injuries are to be avoided. Moreover, the way in which the trolley decelerates in the impact, and the damage inflicted by the test vehicle to the deformable barrier, indicate how efficiently the two partners have interacted. A vehicle which leads to extremely high trolley decelerations or which causes very severe localized deformation is said to exhibit poor 'compatibility'. In the real world, such vehicles may not absorb their own energy as efficiently as they should and pose a threat to other road-users.

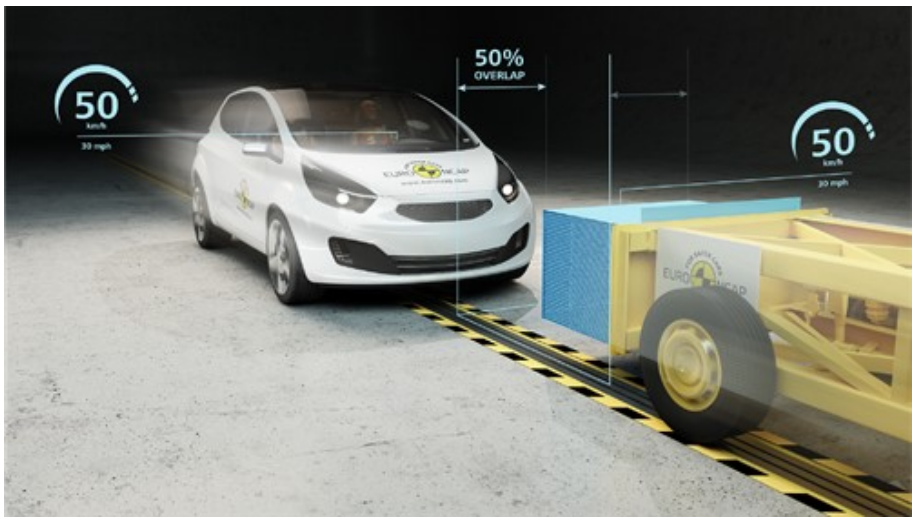


*Figure 2 MPDB test*

**Full rigid barrier test** is a frontal impact test against a rigid wall with 100% overlap (full vehicle width), 0-degree impact angle and vehicle speed equal to 50 km/h. A 5$^{th}$ percentile female frontal impact dummy is seated in the front driver's seat and in the rear passenger side seat. This test places high demands on the restraint systems in front and rear seating positions. Strict limits are placed on the decelerations of the chest and

on the degree of chest deflection and this, in turn, encourages manufacturers to fit more sophisticated restraints. The test complements the moving progressive deformable barrier test as a balance must be found between a restraint system that is stiff enough to restrain a male dummy in the offset test and one that is compliant enough not to put injuriously high deceleration forces on a small female.


*Figure 3 FW test*

**Side mobile barrier test** is a lateral impact test in which the vehicle tested is stationary and it is hit perpendicularly by the AE-MDB barrier bolted to a 1400 kg trolley that travels at 60 km/h. A side impact dummy representing an average male is put in the driver's seat and child dummies are placed in child restraint systems in the rear. The test ensures that there is adequate protection of the critical body regions. This has driven the strengthening the structures of vehicles around the B-pillar (between the doors), the fitment of side impact or curtain airbags in cars but also the development of less obvious energy-absorbing structures in seats and door panels. The timing and deployment of airbags must be very carefully controlled to ensure that they provide the greatest protection possible.

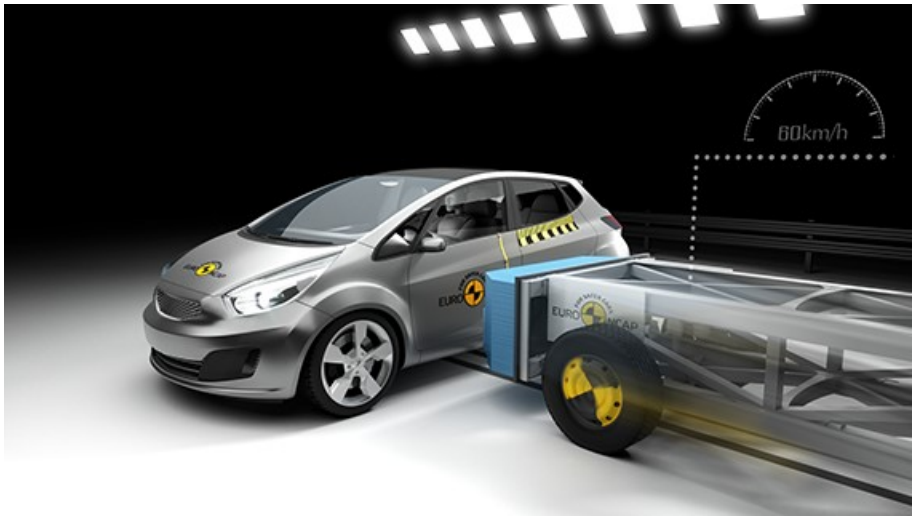


*Figure 4 MD test*

**Side pole test** consists in a lateral impact against a rigid pole. The vehicle travels at 32 km/h and will hit the pole at a slight angle compared to the perpendicular. Where a vehicle is equipped with a centre airbag to protect against the front seat occupants hitting each other, two average male side impact dummies are placed in the front seats. Where there is no centre airbag, single dummy is placed on the driver's seat.

This is a very severe test of a car's ability to protect the driver's head. As the loading on the car is so localised, deformation can be very high and the pole can penetrate deeply into the passenger compartment. Without effective protection, the pole would strike the head resulting in serious or potentially fatal injuries. Head protection airbags – often curtain airbags mounted above the side windows but sometimes seat-mounted thorax/head airbags – have become a common solution but great care is needed to ensure effective performance of such devices.


*Figure 5 PO test*

**Far side test** is done mounting the body-in-white on a sled and then propelling it via a pneumatic cylinder at a 75-degree angle. The sled replicates the accelerations experienced by the vehicle in the side and pole tests, exposing a single dummy, seated on the far-side. The 'excursion' of the dummy - the extent to which the dummy moves towards the impacted side of the vehicle - is measured. At the same time, the dummy itself measures forces and decelerations, most importantly in the head and neck but also in the chest and abdomen, and a score is calculated from these measurements.

*Figure 6 Far side test*

**Whiplash tests** the ability of the restrain system to avoid sudden acceleration in the neck following a moderate rear impact. The dummy and the seat (with seatbelts, pretensioners and load limiter) are mounted on a sled and they are propelled at 16 km/h and at 24 km/h afterword. The dynamic sled tests indicate how effectively the seat and

head restraint operate to provide whiplash protection in typical crash scenarios.

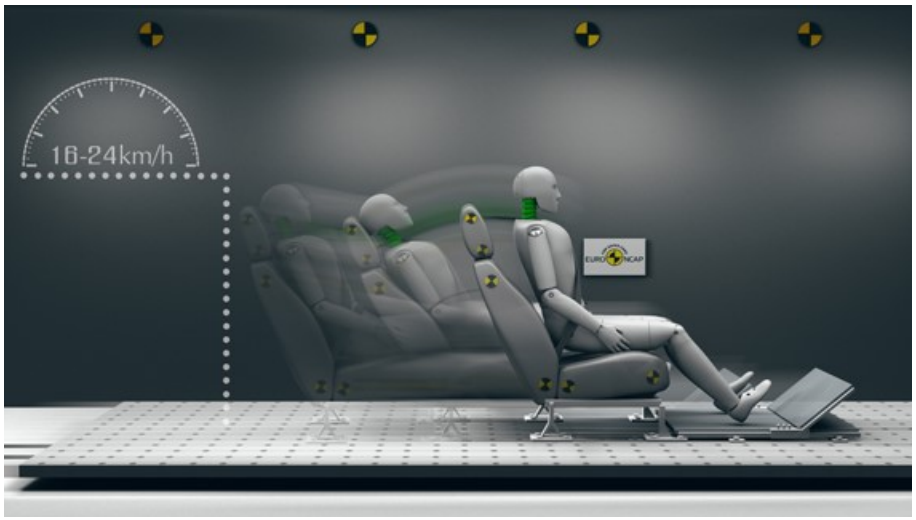


*Figure 7 Whiplash test*

**Rescue and extrication**, introduced in 2020, will assess the after-crash safety of the vehicle, evaluating the force required to open the door, to unlatch the seatbelt. Furthermore, due to the increased complexity and resistance of car structures, car manufacturers are rewarded if they provide information to first-responders through a rescue sheet so that high-voltage systems and high-strength steel can be quickly recognized.

In the constant pursuit of vehicle safety, Euro NCAP, as said, introduced in 2020 a new frontal impact test, the Moving Progressive Deformable Barrier test that replaced the Offset Deformable Barrier Test. A part from the different configuration of the tests (stationary vs moving barrier), the new protocol prescribes a brand-new barrier.

## 3. MPDB vs ODB

MPDB and ODB frontal crashes are designed to simulate an impact with an approaching vehicle. This category of crashes is the most dangerous and so they are used to assess the behaviour and the energy absorption capability of the vehicle structure. In fact, in both cases only one side of the car is loaded (50% overlap for MPDB and 40% for ODB) and the goal is to prevent any intrusions in the passenger compartment. It is also important to keep the position of pedals and steering wheel as stable as possible because the steering wheel supports the driver airbag and the lower dashboard the knee airbag. If airbags are deployed in a position different from the designed one, they can be ineffective or sometime even dangerous.

Another geometric measure to be considered is the position of hinges and locking mechanism of the doors to ensure that after a crash the door can be opened easily.

Biomechanical data are recorded during the crash event through acquisition channels and data are analyzed to compare with reference thresholds to assign scores and concur in the definition of final rating.

The new frontal crash protocol has been introduced to replace Offset Deformable Barrier test, a procedure that has been used since the foundation of the association and uses an outdate barrier for today's standards. Indeed, the Offset deformable barrier has been designed for the vehicles in the 90s, which had much lower stiffness and lower mass, providing a moderate energy intensity. In fact, in recent crash tests this barrier will very often bottom out and let the vehicle hit the rigid wall behind.

The offset deformable barrier is constituted by two types of honeycomb blocks, the main one is a 1000 x 650 x 450 mm honeycomb block with a static crushing resistance of 0.345 MPa and the bumper block, placed in front of the main one, is a 1000 x 330 x 90 mm with static plateau stress of 1.723 MPa. An aluminium sheet, 0.81 mm of thickness, is glued to three faces of the main block and a similar one is glued to the front face of the bumper block.

*Figure 8 Offset Deformable Barrier*

So, the progressive deformable barrier is designed to be a much stiffer barrier, able to absorb a lot more energy. The new protocol prescribes also a moving trolley weighting 1400 kg and travelling at 50 km/h to evaluate the vehicle to vehicle compatibility.

In fact, when a vehicle crashes into a stationary deformable barrier, it is an equivalent case of two cars with identical masses crashing together, while by designing a frontal impact with a moving barrier you are able to test the vehicle against an average car, with the advantage of having homogeneous and repeatable results.

The compatibility assessment is justified by the spread of vehicle classes with very different masses and geometries (height for example) that will lead to poor correlation between vehicle to vehicle crashes and crash test with stationary barriers.

The trolley is designed to be very rigid in order to avoid any deformation and to be easily reusable. All the dimensions are here reported and great emphasis has to be placed on the correct positioning of the center of gravity and hence on the weight balance.

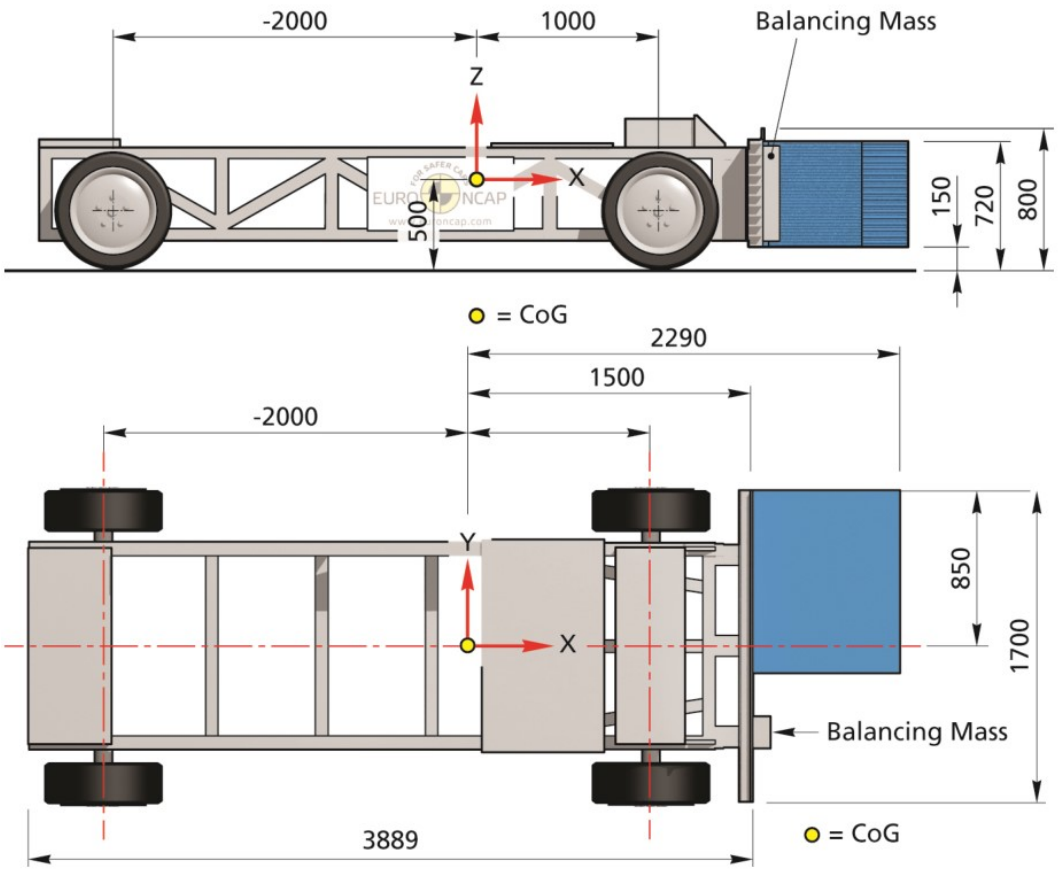


*Figure 9 Trolley specifications*

The progressive deformable barrier is bolted to the trolley and it is constituted by three main blocks of different stiffness. Each block is glued with a two-part polyurethane adhesive to two aluminum sheets of different thickness. Indeed, for the intermediate sheets 5754 H111 aluminum, 0.5 mm thick is prescribed, for the back plate a couple of flanges are included and the material is manufactured from aluminum of series AlMg2 to AlMg3 with hardness between 50 and 67 HBS and a thickness of 3 mm. The contact plate is from 1050A H24 aluminum and 1.5 mm thick and moreover twenty 6.2mm holes are drilled through the contact plate to accommodate blind rivets. Finally, the cladding is manufactured from 5754 H22 aluminum with a thickness of 0.8 mm and it have to accommodate the aforementioned holes to bond with the contact plate.

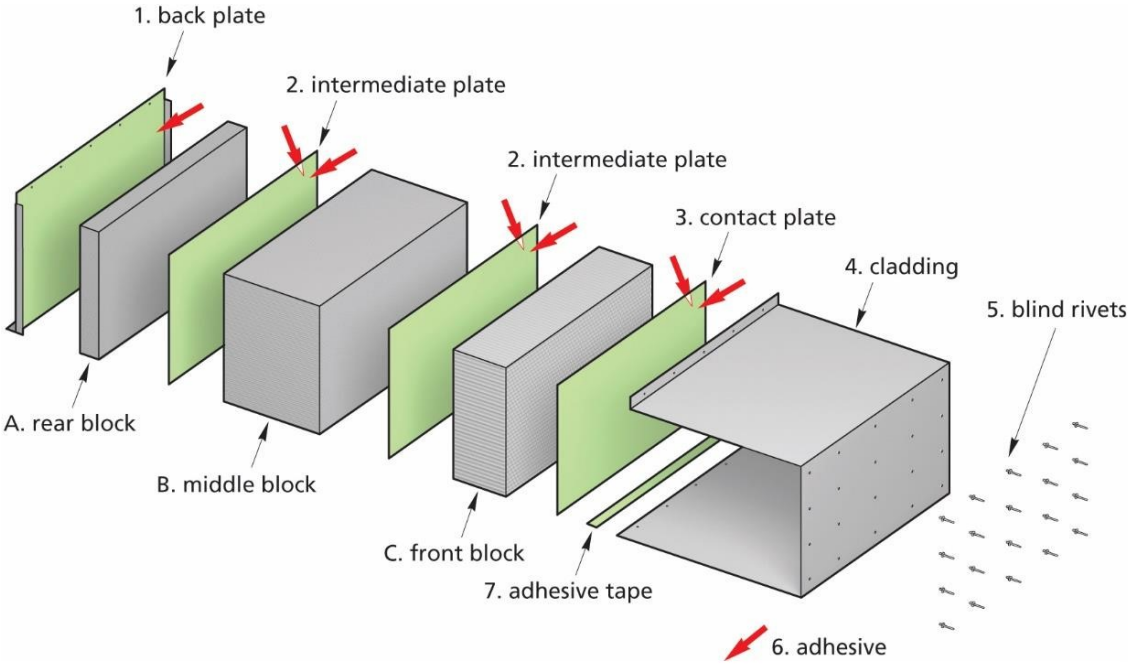


*Figure 10 Progressive Deformable Barrier exploded view*

The honeycomb blocks are made of 3003 aluminum and have two equal dimensions, width and height, respectively 1000 and 568 mm.

The front block, 250 mm deep, has cell size of 19.1 mm and the static crush strength is between 0.308 and 0.342 MPa, while the rear block is 90 mm deep and its cells of 6.35 mm provide a static crushing stress between 1.540 and 1.711 MPa.

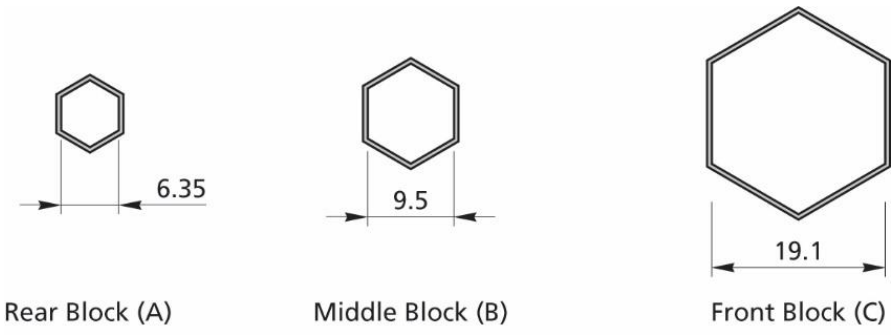


*Figure 11 Blocks' cell dimension*

The middle block is 450 mm deep and has cell size of 9.5 mm. Unlike the other two blocks, the middle one has increasing stiffness, made possible through a continuous thickness change along the depth of the block. This is done manufacturing the block with the maximum foil thickness and then dipping it slowly in an acid solution that will erode the aluminium. Due to the different exposure time to the acid solution a continuously variable thickness honeycomb block is obtained. The increasing crush strength has to be

included in the prescribed static corridor here reported.

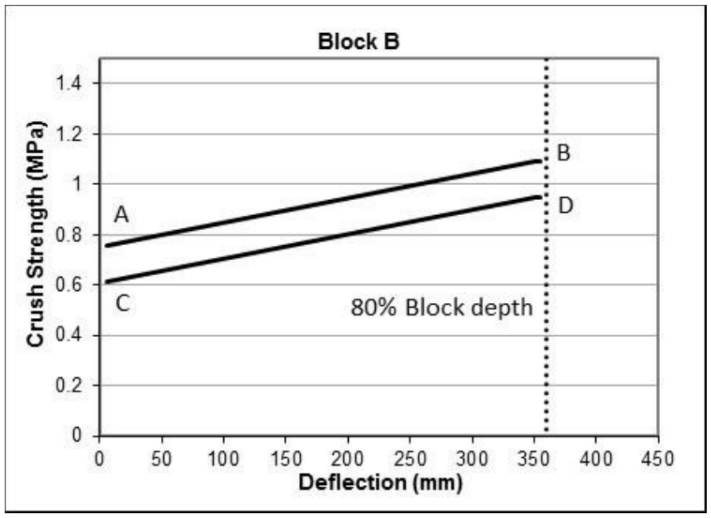


| | Crush | Deflection |
|---|---|---|
| A | 0.756MPa | 6mm |
| B | 1.090MPa | 350mm |
| C | 0.616MPa | 6mm |
| D | 0.950MPa | 350mm |

*Figure 12 Middle block static corridor*

Finally, the entire barrier is bolted on a rigid wall and dynamically tested. A trolley, very similar to the one used in the MPDB test, weights 1300 kg, travels at 60 km/h and is equipped with a rigid tubular frame impactor, that simulates the vehicle crash structures. All the dimensions of the trolley and the barrier-trolley alignment measurements are reported in the technical bulletin but the barrier can only be homologated for crash tests if the force, obtained multiplying the trolley mass by its acceleration recorder by the instrument, is included in the dynamic crash corridor.

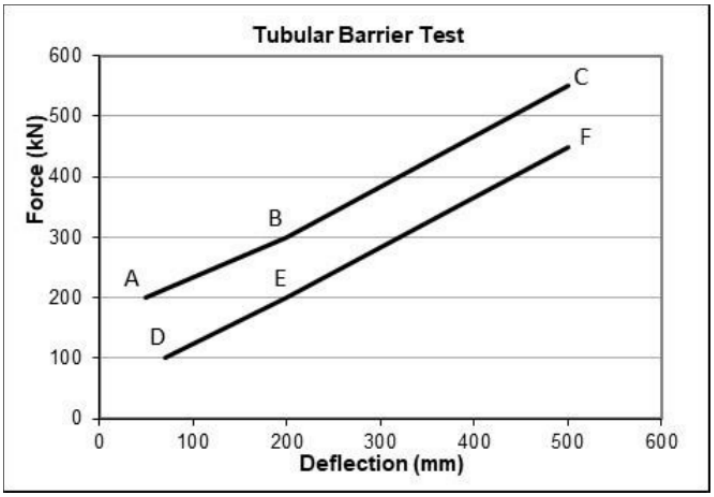


| | Force | Deflection |
|---|---|---|
| A | 200kN | 50mm |
| B | 300kN | 200mm |
| C | 550kN | 500mm |
| D | 100kN | 70mm |
| E | 200kN | 200mm |
| F | 450kN | 500mm |

*Figure 13 Full barrier crash corridor*

## 4. Aluminium honeycomb characteristics

There are five basic ways of manufacturing honeycomb: adhesive bonding, resistance welding, brazing, diffusion bonding and thermal fusion. Among these methods, most common manufacturing method is adhesive bonding. Resistance welding, brazing and diffusion bonding are only used for cores to be used at very high temperatures. There are two basic methods of manufacturing honeycomb core by adhesive bonding:

1. Expansion method
2. Corrugation method

A schematic of expansion process for honeycomb core manufacturing is shown in Figure 14. Metallic sheet is cut into specified dimensions and strips of adhesive are printed on it. Adhesive is applied in such a way that adhesive prints on adjacent sheets are shifted by half of the distance between adjacent prints on the same sheet. After solidification and curing of the adhesive, the honeycomb before expansion (or HOBE) block is sliced into required thickness of the core and then is expanded to form honeycombs.

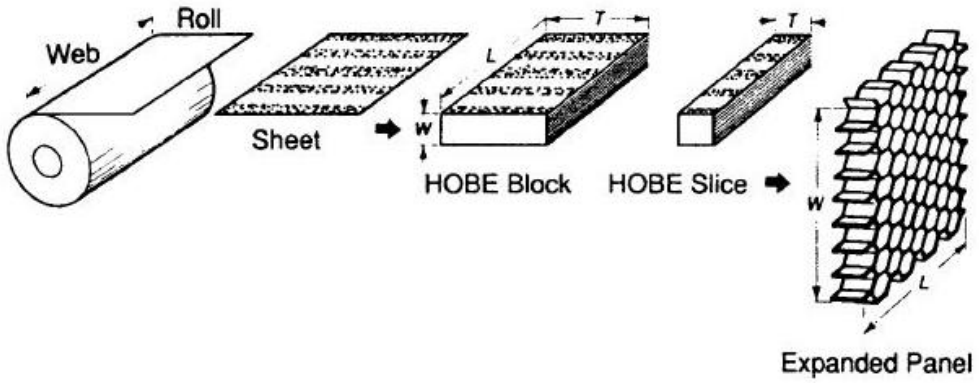


*Figure 14 Expansion method*

Manufacturing of core by corrugation method is shown in Figure 15. In this method corrugations are produced by pressing metallic sheet between toothed rollers. Corrugated sheets are then bonded, brazed or resistance welded to form honeycomb core. This method is generally preferred for high density cores which cannot be

expanded due to thick and strong metallic sheets.

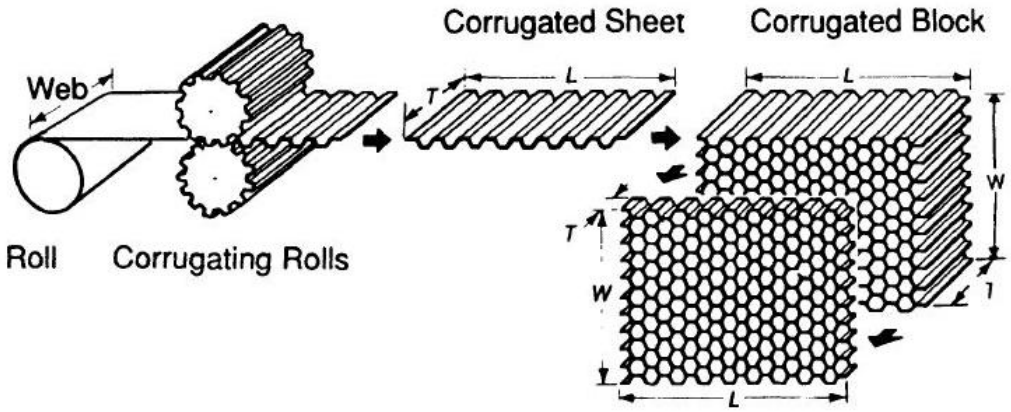


*Figure 15 Corrugated method*

Honeycomb strain stress characteristic during compression makes them attractive for crash energy dissipation. This characteristic exhibits a relatively small linear part (5% max deformation) followed by a flat section with nearly constant stress. During this phase the cells that constitute the material begin to collapse by elastic buckling, plastic yielding or brittle failure, and this collapse proceeds in the material at a nearly constant stress. When most of the cells have collapsed with opposite walls in contact (densification) the stress exhibits a sharp increase.

The density has a large influence on the stress-strain curve. Figure 16 shows that increasing the density the stress corresponding to a given deformation increases but the densification occurs at lower strain. The density change is generated by differences in foil thickness, cell size and their ratio. A paper by Xu, Beynon, Ruan and Lu contains out-of-plane compression for an extended number of honeycomb blocks. Each block is in 9x9 configuration because it is the minimum arrangement to replicate the full-scale behavior of a crash barrier block. Each factor is individually isolated and tested and the characteristic is extrapolated from the curves and that gives a deeper explanation to the increase in resistance with the increase in honeycomb density.

The energy per unit volume absorbed during the deformation is equal to the area under the stress strain curve. Most of the energy is dissipated in the plateau, where the stress

is nearly constant.

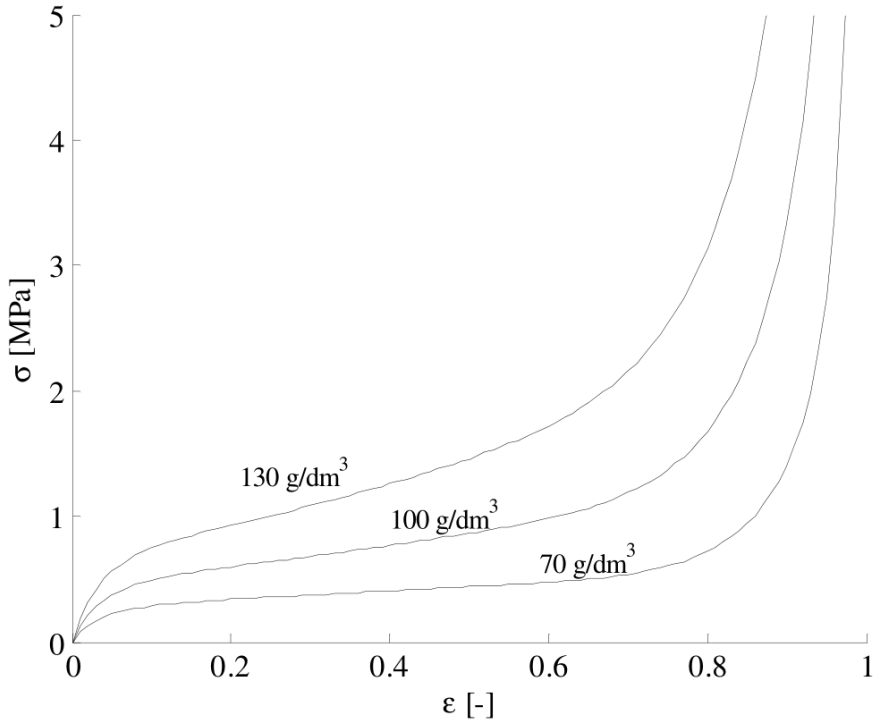


*Figure 16 Stress strain curve of a polymeric foam*

Strain rate is another factor that influence honeycomb behavior but to avoid that in the barriers ventilation holes are made so that air, the main cause of this phenomenon, can escape the blocks.

# 5. LSTC MPDB reference virtual barrier

In order to simulate the honeycomb behaviour a mathematical replication of the barrier, a FEM model, is created. The FEM is a particular numerical method for solving partial differential equations in two or three space variables. To solve a problem, the FEM subdivides a large system into smaller, simpler parts that are called finite elements. This is achieved by a particular space discretization in the space dimensions, which is implemented by the construction of a mesh of the object: the numerical domain for the solution, which has a finite number of points. The finite element method formulation of a boundary value problem finally results in a system of algebraic equations. The simple equations that model these finite elements are then assembled into a larger system of equations that models the entire problem. The FEM then uses variational methods from the calculus of variations to approximate a solution by minimizing an associated error function.

A finite element method is characterized by a discretization strategy (or pre-processing), a solution algorithm, and post-processing procedures.

A discretization strategy is understood to mean a clearly defined set of procedures that cover the creation of finite element meshes, the definition of basis function on reference elements (also called shape functions) and the mapping of reference elements onto the elements of the mesh. Various numerical solution algorithms can be classified into two broad categories; implicit and explicit solvers. These algorithms are designed to exploit the shortage of matrices that depend on the choices of variational formulation and discretization strategy. Postprocessing procedures are designed for the extraction of the data of interest from a finite element solution.

This CAE tool allows to run all the test needed without crashing an actual vehicle against the barrier or during the vehicle development phases when physical prototypes are not yet available. Different possibilities are available to every car manufacturer and safety specialist concerning the virtual barrier model, such as developing the model in-house, using a freely available barrier or one obtained for a fee. One of the free alternatives is the barrier created by LSTC that has been used during this work as well. LSTC is the software house behind LS-Dyna, a vastly used FEM solver for crash simulations. LS-DYNA

is a general-purpose finite element program capable of simulating complex real-world problems. It is used by the automobile, aerospace, construction, military, manufacturing, and bioengineering industries. The code's origins lie in highly nonlinear, transient dynamic finite element analysis using explicit time integration. "Nonlinear" means at least one (and sometimes all) of the following complications:

- Changing boundary conditions (such as contact between parts that changes over time)
- Large deformations (for example the crumpling of sheet metal parts)
- Nonlinear materials that do not exhibit ideally elastic behaviour (for example thermoplastic polymers)

"Transient dynamic" means analysing high speed, short duration events where inertial forces are important. Typical uses include:

- Automotive crash (deformation of chassis, airbag inflation, seatbelt tensioning)
- Explosions (underwater Naval mine, shaped charges)
- Manufacturing (sheet metal stamping)

The honeycomb blocks of the barrier are made with R-tria shell elements with element formulation #4, C0 triangular shell, and the thickness is not the same of the real barrier. Indeed, in order to reduce the elements counts, the cell size is increased to 34.1 mm across all blocks and consequently the thickness is calibrated so that the behaviour is the same. The material used is MAT_PIECEWISE_LINEAR_PLASTICITY from LS-Dyna with material parameters peculiar to 3000-series aluminium.

The outer cladding, the intermediate sheets and the thicker back plate are modelled with shell elements and two plastic materials. The element formulation is #16, fully integrated shell element (very fast), while the material is MAT_PLASTIC_KINEMATIC for the back plate and MAT_PIECEWISE_LINEAR_PLASTICITY for all the other sheets. The glue between plate and block is modelled with equivalent beam elements and MAT_SPOTWELD.

The contact plate in this model is merged with the front portion of the cladding, so that a single 2.3 mm thick entity is present. This component is modelled with a thick shell

instead of a thin shell due to the mesh size to thickness ratio and the material used is MAT_PIECEWISE_LINEAR_PLASTICITY.

This barrier model is very similar to the real one and it has been used as a reference point for this work. The only but important issue with this model is that, with an element count of 2 million, this barrier has a very high simulation cost, meaning that a crash simulation using this barrier needs a significant number of hours and cores to finish.

This is somewhat justified by the fact that the barrier is a deformable entity and as such it will always bring a simulation time penalty. Nevertheless, the goal of this work is to create an equivalent barrier built with solid elements that includes an advanced failure criterion able to model the bottoming of the honeycomb blocks and provides a reasonable simulation time when compared to the reference barrier. This can be useful to reduce simulation time during development stage, when a high number of virtual tests are performed and so this can add up to a great advantage.

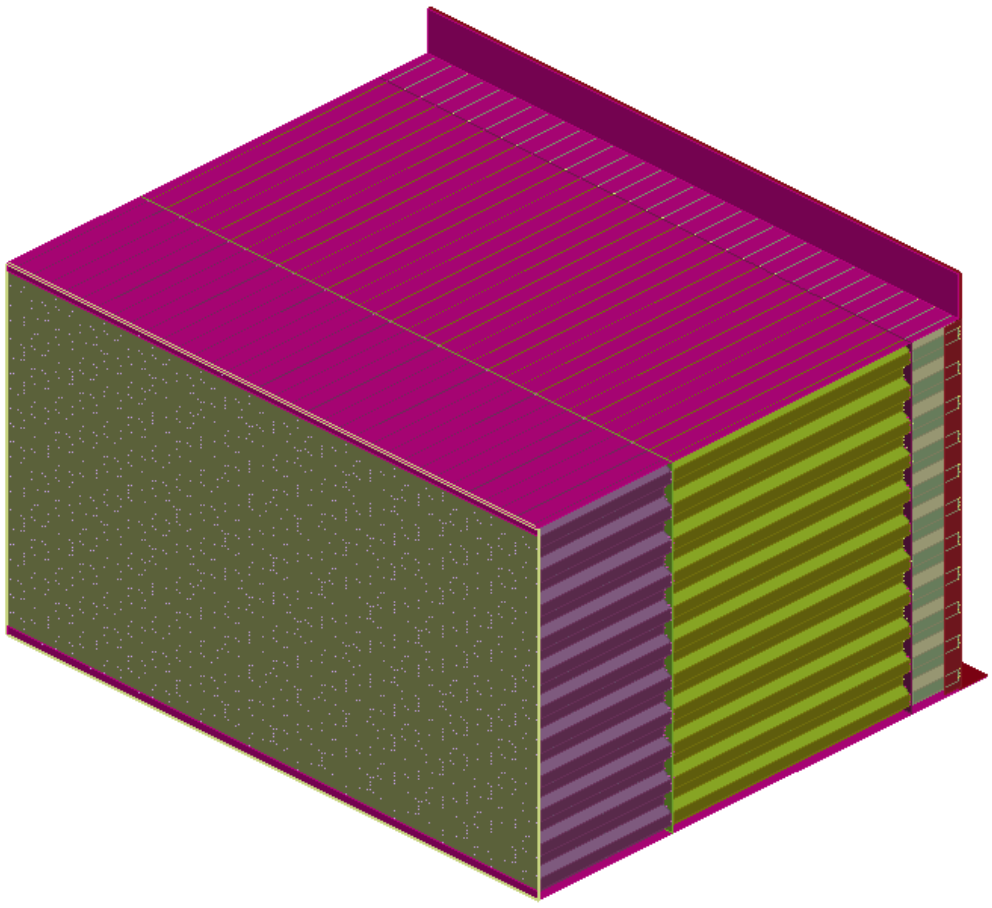

*Figure 17 MPDB virtual model*

## 6. MPDB optimization

In order to find a good solution for creating an efficient and advanced model of barrier, first of all a benchmark analysis of the available models was performed. One of the first attempt with previous crash barrier was conducted using beam elements instead of shell ones. This solution, presented at the 2008 LS-Dyna Conference, proved to be very efficient and effective but it uses an outdated solution to the problem, given that the computational power at disposal of companies has increased massively and that the inability to delete elements would lead to numerical problems such as extremely deformed elements or nodes that manage to escape the contact algorithm.

In the paper presented by Jost, Heubrandtner, Ruff and Fellner, the model was built with Discrete Beam Elements, mimicking the honeycomb geometry, that acts like springs and the material used was MAT_NONLINEAR_PLASTIC_DISCRETE_BEAM.

Starting from detailed tests the aluminium honeycomb model was validated. Special focus was given to realistic global and local deformation behaviour of honeycomb structures. Especially the ability of realistic local failure of the honeycomb structure and a constant time step are major advantages. Moreover, a component validation was done to ensure realistic combined deformation behaviour of honeycomb structures and cladding sheets.

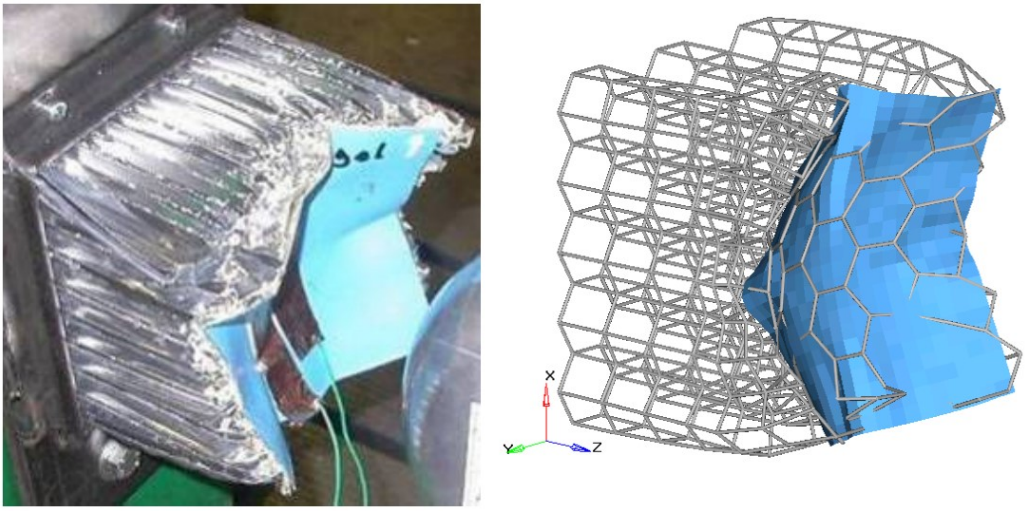


*Figure 18 Component validation in discrete beam model*

Finally, a prototype model of the side impact IIHS barrier has been set up and was validated based on seven load cases with different rigid barriers. Two load cases, the

'rigid rocker' and ‘the three poles' are presented in the paper. In general, the barrier model shows quite good results compared to the tests. Although the aluminium honeycomb model is qualitatively good, special attention has to be given to local phenomena like sheet metal failure and glue failure. To obtain high quality barrier models these local phenomena have to be taken into account. Additional to the IIHS barrier model an ODB demonstrator model has been set up and the real deformation behaviour is well shown by the model. In summary, the discrete beam method ensures high stability even under severe deformation of the honeycomb structure without any problems of numerical instability.

An alternative solution is proposed by Walker, Bruce, Tattersall and Asadi, who used solid elements to model different types of crash barriers. The models obtained are the results of a large number of physical tests in order to correlate correctly the material card MAT_MODIFIED_HONEYCOMB. The tests performed are under three categories, honeycomb, adhesive and full barrier testing. The honeycomb testing includes crush test, angle shear test and piercing test. Adhesive testing include plate pull test for core and plate and also plate shear test for plate.

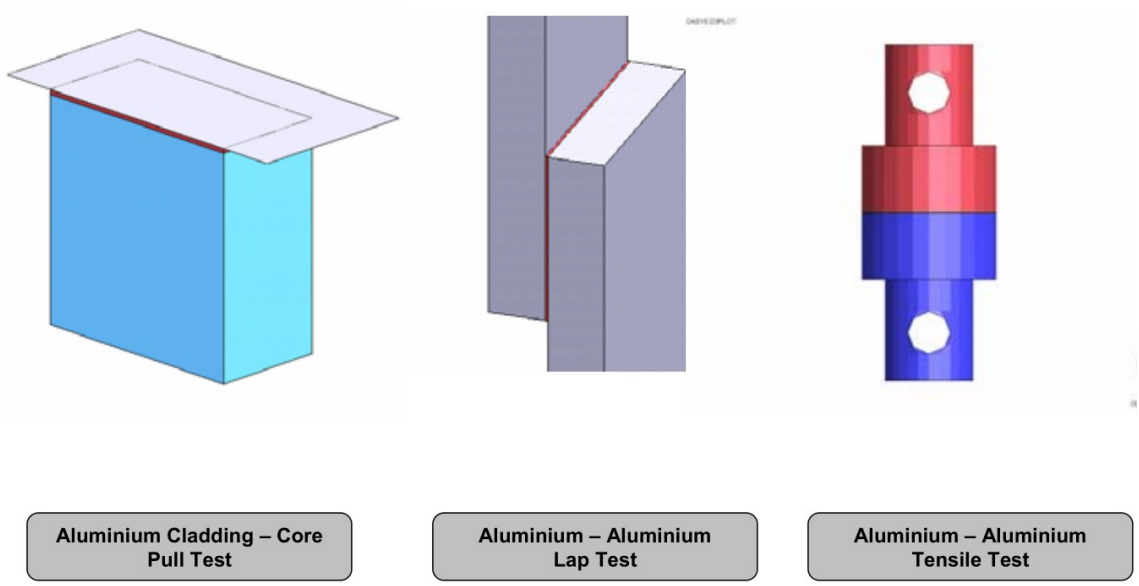


*Figure 19 Adhesive testing in solid element model*

Finally, full barrier testing includes pole, rigid wall, 50% offset wall and rear armature tests. The material card, MAT_126, utilizes the optional second yield surface that considers the effects of off-axis loading and make the material behaviour transversely

isotropic. The results show good correlation between real and virtual barriers for IIHS, NHTSA and AEMBD crash barriers.

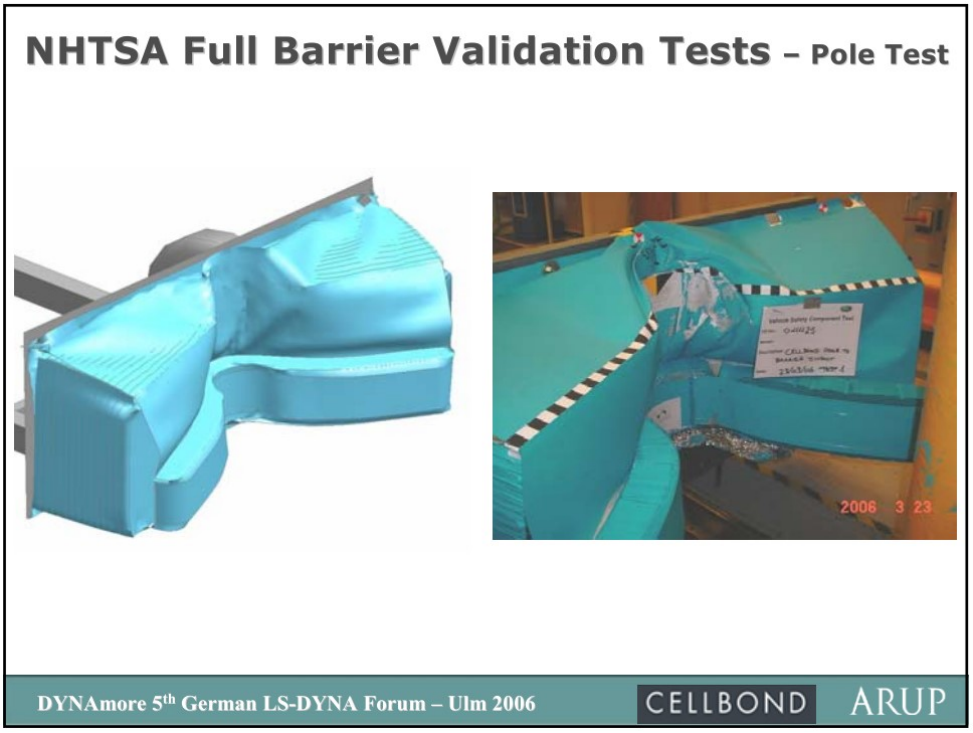


*Figure 20 Full barrier validation in solid element model*

Following these encouraging results, the solution chosen in this thesis is the approximation of a honeycomb cell into a hexahedral element, using a complex material law to match the real behaviour of the barrier. Indeed, among the huge variety of material models in LS-Dyna, all the foams and the honeycomb materials have been considered. In fact, not all the materials are suited to the model because the right one has to cope well with solid elements formulation, it has to allow for large deformations and large volume changes and present an anisotropic behaviour.

Material type 53 is used for low density, closed cell polyurethane foam. The behaviour is isotropic and the air trapped is modelled as added stiffness, so it can not be used in the crash barrier model. Material type 63 is dedicated to crushable foam with optional damping and tension cut-off. This material could be used but only one direction can be specified, with no mention to anisotropic behaviour. Very similarly to 63, material type 75 is modelling isotopic crushable foams and uniaxial and triaxial test data are used to describe the behaviour. A strong candidate is material type 142, used for extruded foam materials that are transversely isotropic, crushable and of low density with no significant

Poisson effect. But this material is usually used for polymeric foams that absorb low and medium velocity impacts.

When available, the modified versions of the listed materials are analysed, but since the material law is similar, they proved to be unsuitable as well.

Eventually the material chosen is Material Type 126, MAT_MODIFIED_HONEYCOMB. The major use of this material model is for aluminium honeycomb crushable foam materials with anisotropic behaviour. Here nonlinear elastoplastic material behaviour can be defined separately for all normal and shear stresses, which are considered to be fully uncoupled.

For solid element formulations 1, constant stress solid element, the behaviour before compaction is orthotropic where the components of the stress tensor are uncoupled, i.e., an a-component of strain will generate resistance in the local a-direction with no coupling to the local b and c directions. The elastic moduli vary from their initial values to the fully compacted values linearly with the relative volume:

$$E_{ij} = E_{ij\,u} + \beta(E - E_{ij\,u})$$

Where

$$\beta = \max\left[min\left(\frac{1-V}{1-V_f}, 1\right), 0\right]$$

V is the relative volume, $V_f$ is the relative volume at which the material is considered fully compressed, $E_{ij\,u}$ is the uncompressed material stiffness in the ij direction.

At the beginning of the stress update we transform each element's stresses and strain rates into the local element coordinate system. For the uncompacted material, the trial stress components are updated using the elastic interpolated moduli according to:

$$\sigma_{ij}^{n+1^{trial}} = \sigma_{ij}^{n} + E_{ij}\Delta\varepsilon_{ij}$$

each component of the updated stress tensor is checked to ensure that it does not exceed the permissible value determined from the load curves, e.g., if

$$\left|\sigma_{ij}^{n+1^{trial}}\right| > \lambda\sigma_{ij}(\varepsilon_{ij})$$

Then

$$\sigma_{ij}^{n+1} = \sigma_{ij}(\varepsilon_{ij})\frac{\lambda\,\sigma_{ij}^{n+1^{trial}}}{\left|\sigma_{ij}^{n+1^{trial}}\right|}$$

The parameter λ is either unity or a value taken from the load curve number, LCSR, that defines λ as a function of strain-rate.

The element formulations easily compatible with this material are #0, #1, #9. Element formulation 1 is the default one for solid elements, constant stress solid element, while formulations 0 and 9 are 1-point corotational element applicable only to MAT_MODIFIED_HONEYCOMB that behave essentially as nonlinear springs so as to permit severe distortions sometimes seen in honeycomb materials. As explained in the next chapters, some experimentation has been done on the element formulation and eventually the more stable #1 formulation has been adopted.

# 7. Material characterization in scale model

Once MAT_MODIFIED_HONEYCOMB has been chosen, the characterization process was split into scale-tests and full-scale tests and it was compared to a reference model built with shell elements and the exact geometry dimensions of a real MPDB barrier. That means that for the C block the cell size is 19.1 mm and the foil thickness is 40 µm. The material used was MAT_PIECEWISE_LINEAR_PLASTICITY with properties of a 3000 series Aluminium and the mesh used was 5 mm quads with fast fully integrated formulation.
Analysing the material card, some of the important parameters were the honeycomb elastic stiffnesses and the load curves to be followed during the deformation in all compression and shear directions. For this reason, the scale-tests were divided into three obvious sections: linear range, plastic range and finally tearing.

## 7.1 Elastic range

For the linear range modelling a so-called Unit Cell Method, described in a paper by F. Ernesto Penado, was used. This system is originally used for the definition of elastic properties for honeycomb sandwich materials and it consists in the analysis of a 1/8 of a cell. In fact, by properly applying constraints and displacements in the model, you are able to simulate the behaviour of a cell and finally the stiffness is the result of the reaction force found divided by the known applied displacement. This procedure is repeated for each stiffness to be found because a different set of constraints and displacements has to be assigned.

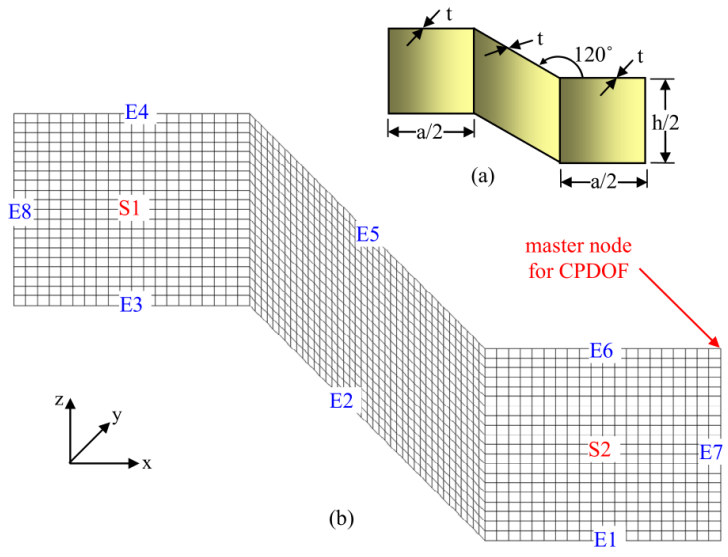


*Figure 21 unit cell method dimensioning*

**Boundary conditions needed for the proper modeling a 1/8 segment of a unit cell**

| Location (see **Figure 3(b)**) | Boundary conditions† | | | | | | | | |
|---|---|---|---|---|---|---|---|---|---|
| | $E_x$, $\nu_{xy}$ and $\nu_{xz}$ | $E_y$, $\nu_{yx}$ and $\nu_{yz}$ | $E_z$, $\nu_{zx}$ and $\nu_{zy}$ | $G_{xy}$ | $G_{yx}$ | $G_{xz}$ | $G_{zx}$ | $G_{yz}$ | $G_{zy}$ |
| E1 | SZ | SZ | SZ | SZ | SZ | AZ | AZ | AZ | AZ |
| E2 | SZ | SZ | SZ | SZ | SZ | AZ | AZ | AZ | AZ |
| E3 | SZ | SZ | SZ | SZ | SZ | AZ | AZ | AZ | AZ |
| E4 | $u_z$ uniform (CPDOF) | $u_z$ uniform (CPDOF) | $u_z = 1$ | free | free | $u_x = u_y = 0$ | $u_x = 1$ $u_y = u_z = 0$ | $u_x = u_y = 0$ | $u_y = 1$ $u_x = u_z = 0$ |
| E5 | $u_z$ uniform (CPDOF) | $u_z$ uniform (CPDOF) | $u_z = 1$ | free | free | $u_x = u_y = 0$ | $u_x$=1 $u_y = u_z = 0$ | $u_x = u_y = 0$ | $u_y = 1$ $u_x = u_z = 0$ |
| E6 | $u_z$ uniform (CPDOF) | $u_z$ uniform (CPDOF) | $u_z = 1$ | free | free | $u_x = u_y = 0$ | $u_x = 1$ $u_y = u_z = 0$ | $u_x = u_y = 0$ | $u_y = 1$ $u_x = u_z = 0$ |
| E7 | $u_x = 1$ | $u_x$ uniform (CPDOF) | $u_x$ uniform (CPDOF) | $u_y = 1$ | AX | $u_z = 1$ $u_x = u_y = 0$ | AX | SX | SX |
| E8 | SX | SX | SX | AX | AX | AX | AX | SX | SX |
| S1 | SY | SY | SY | AY | AY | SY | SY | AY | AY |
| S2 | $u_y$ uniform (CPDOF) AR = 0 | $u_y = -1$ AR = 0 | $u_y$ uniform (CPDOF) AR = 0 | AY | $u_x = -1$ $u_y = u_z = 0$ | SY | SY | $u_z = -1$ $u_x = u_y = 0$ | AY |

†SX, SY, SZ = symmetry conditions with respect to a plane perpendicular to the X, Y, Z axis; AX, AY, AZ = anti-symmetry conditions with respect to a plane perpendicular to the X, Y, Z axis; $u_x$, $u_y$, $u_z$ = displacement in the $x$, $y$, $z$ direction; CPDOF = coupled degrees of freedom; AR = all rotations.

*Figure 22 unit cell method boundary conditions*

In particular SX, symmetry conditions with respect to a plane perpendicular to X axis, means that the translation in X axis has to be constrained, as well as the rotations about Y and Z. while AX, anti- symmetry conditions with respect to a plane perpendicular to X axis, means that the translations in Y and Z are constrained and likewise is the rotation about X. The uniform translation, obtained via the coupled degree of freedom in Abaqus, here in LS-Dyna has been obtained constraining the rotation perpendicular to the edge and to the prescribed uniform motion.

The imposed displacement is a 1 mm ramp and in nearly all the cases it caused a plastic deformation. In order to consider the elastic response of the material, only the first region is considered. So, the force and the displacement used to compute the stiffness are those at t=2.5 ms in the case below, which is the curve output from $G_{xz}$ calculation. Considering that the motion speed is constant and equal to 1/90 m/s, the displacement is obtained multiplying the time instant by the speed, 0.028 mm in this case.

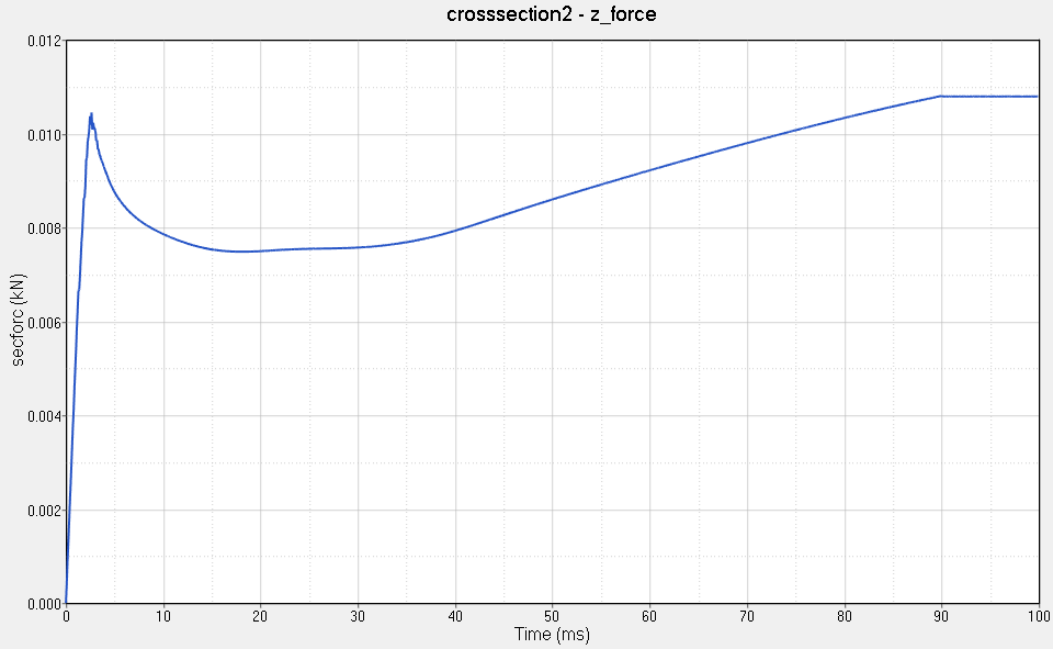


*Figure 23 Gxz calculation output curve*

Now to obtain the desired stiffnesses a simple division is made:

$$E_i = \frac{\sigma_i}{\varepsilon_i} = \frac{F_i/A_i}{u_i/L_i}$$

And

$$G_{ij} = \frac{\tau_{ij}}{\gamma_{ij}} = \frac{F_j/A_i}{u_j/L_i}$$

Where $F_i$ and $u_i$ are the aforementioned values of force and displacement in i-direction, $A_i$ is the projected area of the whole cell on a plane perpendicular to i-direction and $L_i$ is the length of the entire cell in i-direction.

In the following table the measurements are summarized:

| | Ex | Ey | Ez | Gxy | Gxz | Gyz |
|---|---|---|---|---|---|---|
| F[N] | 0.042 | 0.052 | 83.5 | 0.00187 | 10 | 10.4 |
| t[ms] | 90 | 33 | 1.2 | 4 | 2.5 | 1.68 |

| u[mm] | 1.000 | 0.367 | 0.013 | 0.044 | 0.028 | 0.019 |
|---|---|---|---|---|---|---|
| A[mm2] | 363.66 | 629.92 | 318.06 | 363.66 | 363.66 | 629.92 |
| L[mm] | 32.98 | 19.04 | 19.1 | 32.98 | 32.98 | 19.04 |
| **E[MPa]** | **0.0038** | **0.0043** | **376.07** | **0.0038** | **32.65** | **16.84** |

To confirm these values, the theoretical formulas explained in Gibson-Ashely's book have been used. Considering a single cell, the elementary moment and deflection are computed and then the stiffness is obtained as the ratio between the two. So, for the stiffness in x direction the formula is:

$$E_x^* = E_s \left(\frac{t}{l}\right)^3 \frac{cos\theta}{(h/l + sin\theta)\sin^2\theta}$$

Where $E_s$ is the solid material Young modulus, t is the foil thickness, l is the length of the oblique edge of the cell, h is the length of the vertical edge of the cell and $\theta$ is the angle between the vertical and the oblique edge of the cell.

The elastic modulus in y direction is instead:

$$E_y^* = E_s \left(\frac{t}{l}\right)^3 \frac{(h/l + sin\theta)}{\cos^3\theta}$$

The resulting formulas can be simplified in case of regular hexagonal cell with uniform wall thickness, that is if the ratio h/l is equal to 1, the angle $\theta$ is equal to 60 degree and the foil thickness does not change. The two formulas are equivalent with these assumptions and equal to:

$$E_x^* = E_y^* = 2.3\, E_s \left(\frac{t}{l}\right)^3$$

The other formulas, simplified for the geometry of the cell used, are as follow:

$$G_{xy}^* = 0.57\, E_s \left(\frac{t}{l}\right)^3$$

$$E_z^* = 1.15\, E_s \left(\frac{t}{l}\right)$$

$$G_{xz}^* = G_{yz}^* = 0.577\, G_s \left(\frac{t}{l}\right)$$

Substituting the various parameter, the theoretical values are computed. Although the values are not exactly the same, the order of magnitude is the same and this give the confidence of the results found via numerical simulations.

| Ex [MPa] | Ey [MPa] | Ez [MPa] | Gxy [MPa] | Gyz [MPa] | Gxz [MPa] |
|---|---|---|---|---|---|

| | | | | | |
|---|---|---|---|---|---|
| 0.008 | 0.008 | 293.12 | 0.0019 | 55.10 | 55.10 |

## 7.2 Plastic Range

In order to model the plastic range, compression and shear tests were performed on the reference model. A portion of the barrier was taken, precisely a 9x9 array of cell because, as expressed in the paper by Shanqing Xu, John H. Beynon, Dong Ruan and Guoxing Lu, this setup is the least cell units one to approximate correctly the full-scale behaviour of the barrier. The block was put between two big plate of rigid metallic material and, in order to avoid dynamic behaviour in the material, the velocity of the moving plate was 0.1m/s and an exponential increase in velocity in the first 5 ms was necessary to avoid instabilities.

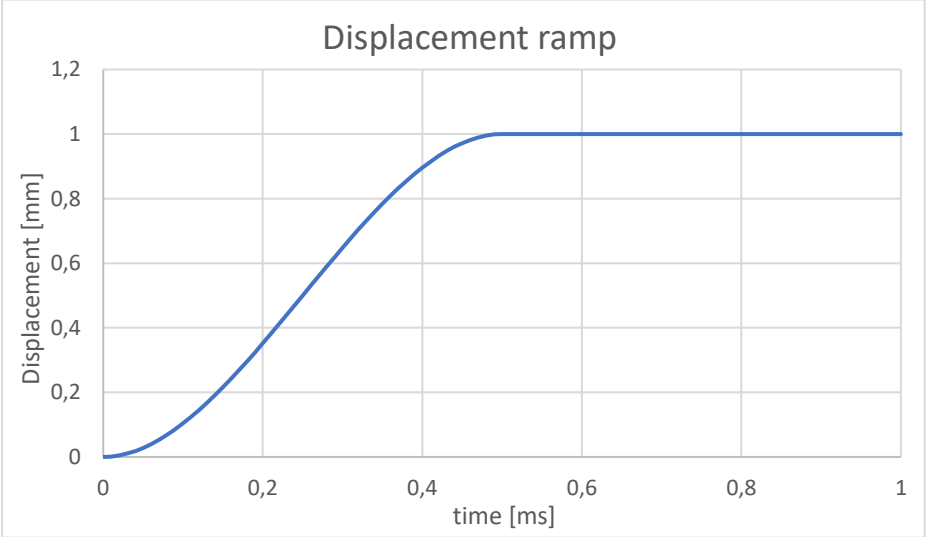


*Figure 24 Exponential input displacement ramp*

The simulation setup of the compression tests is straightforward, with the only attention being to constrain the plates movements not interested in the test. This means that for a compression in the z axis, any displacements in x and y axes and all the rotations should be locked. Instead for shear tests the honeycomb block is constrained to the plates through the card *CONSTRAINED_EXTRA_NODE and the moving plate is allowed to move in the direction perpendicular to the imposed movement in order to avoid any tensile stress during the test. This means that in a xz shear test, z being the imposed displacement, the x translation is free, while y translations and all the rotations are locked.

Now that the material reaction forces are obtained, these curves are discretized and used as the other input parameters needed by the *MAT_MODIFIED_HONEYCOMB material card and are shown below.

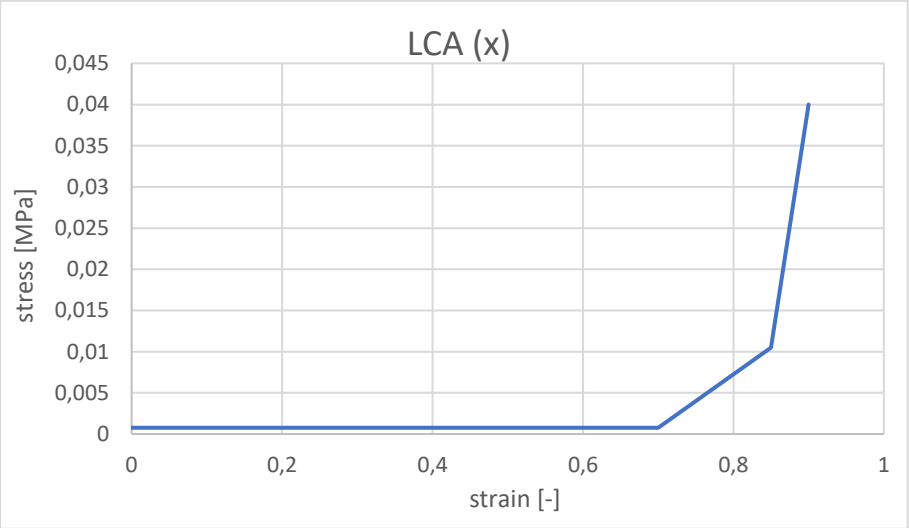


*Figure 25 x-direction input curve*

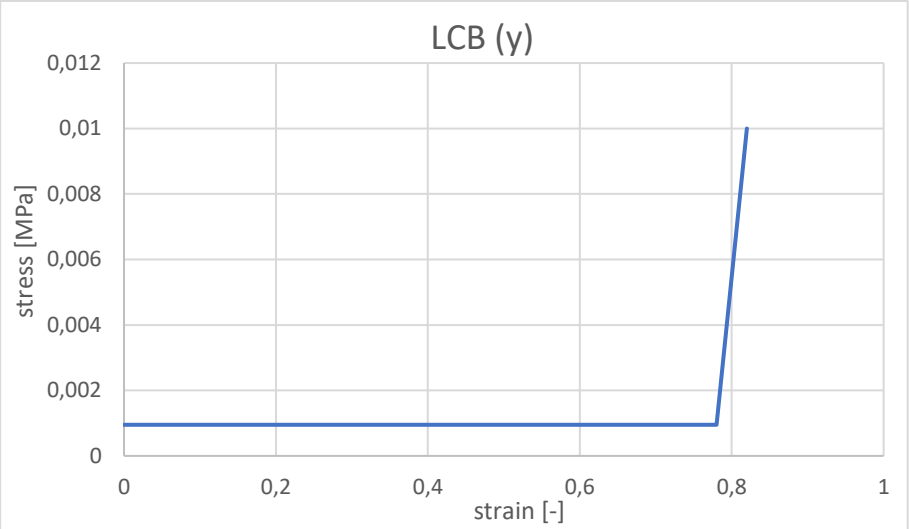


*Figure 26 y -direction input curve*

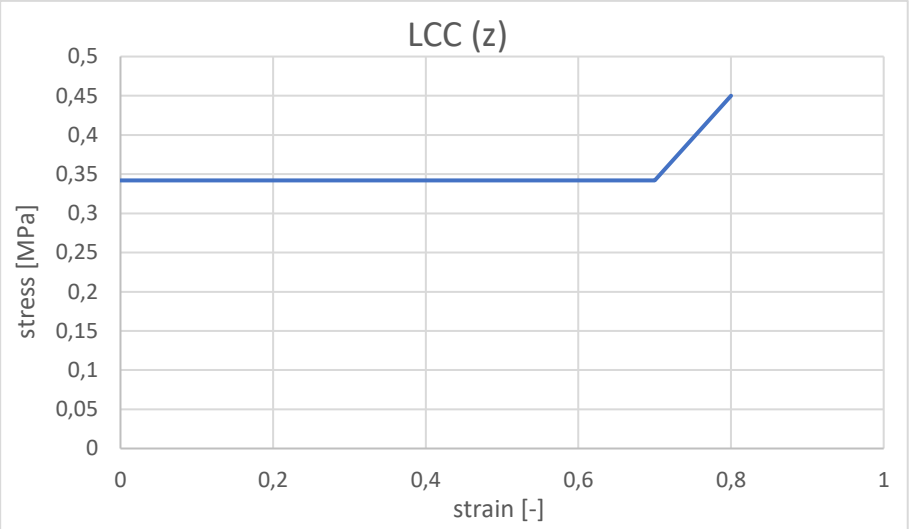


*Figure 27 z-direction input curve*

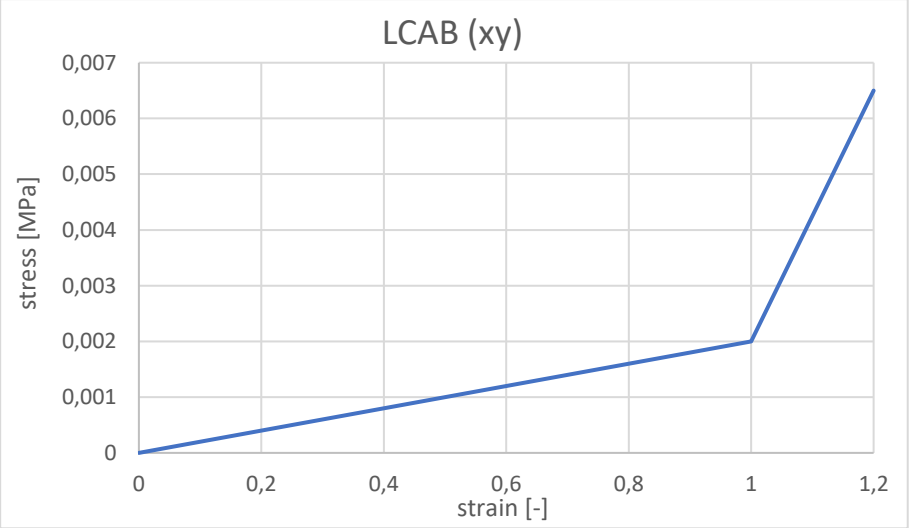


*Figure 28 xy-direction input curve*

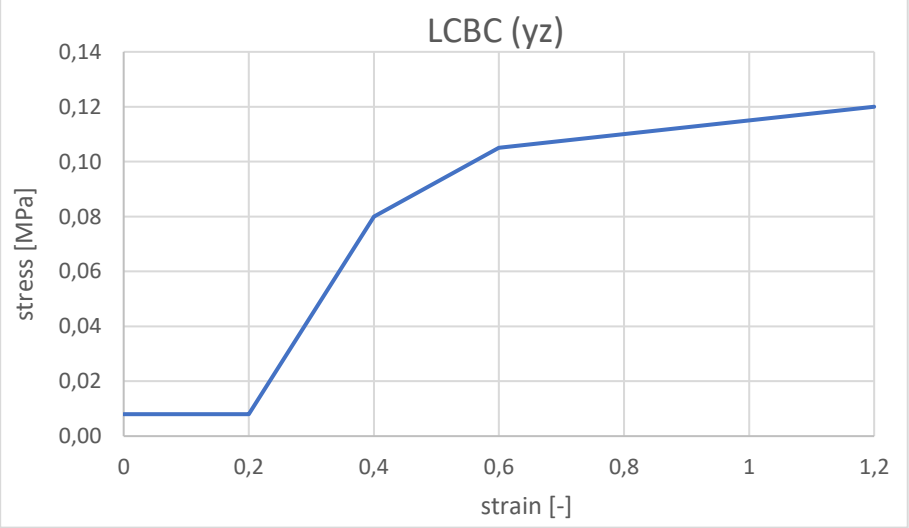


*Figure 29 yz-direction input curve*

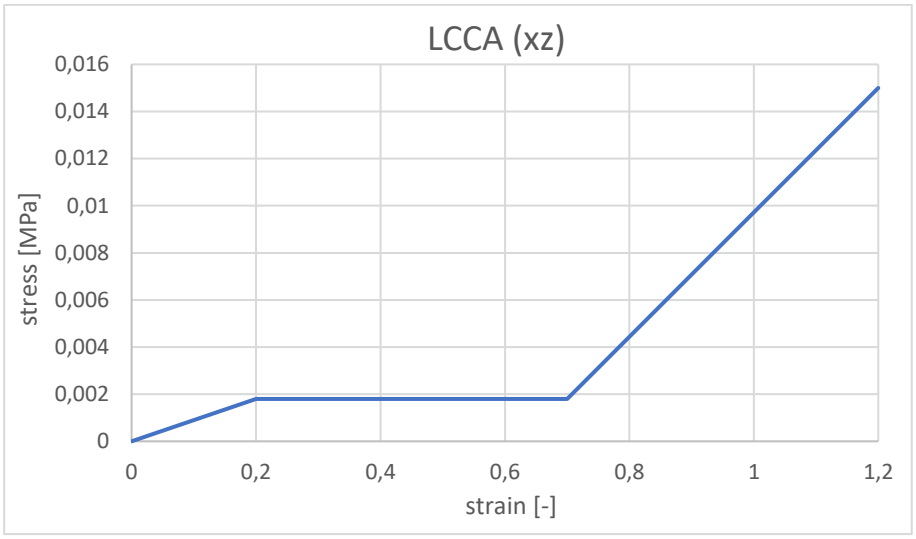


*Figure 30 xz-direction input curve*

The first issue encountered is that the model run into computational instabilities likely due to the low density of the hexahedral model. As a matter of facts, being the hexahedral model a continuum cube of material, it has to take into consideration also the air inside the honeycomb and so the density of this model, to match the mass, is in the $10^{-8}$ order of magnitude instead of $10^{-6}$ as for solid aluminium. This downside is accounted for by increasing the solid material Young's modulus in the material card and, even if the computation timestep is negatively affected, the model is stable and does not affect the reaction force curve.

The other issue encountered is on the shear tests, mostly due to the geometric configuration of the test and to the element formulation used. Indeed, in the hexahedral model, the block tends to deform only the rows of material close to the plates and to rotate the rest of the block so that the reaction force is really low and it does not correlate well with the shell model.

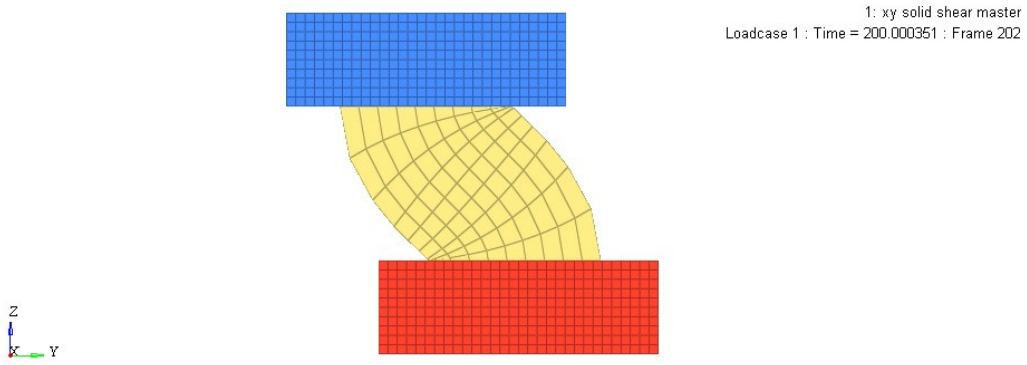


*Figure 31 xy shear test with element formulation #9*

This issue however is inherited by the solid element formulation #9, because when trying with formulation #1, all the rows of the block reacted to the shear deformation in the same manner but the resulting force turned out to be higher than with formulation #9, but still much lower and with different trend respect to the shell.

To solve the problem another test configuration is used: considering only two rows of the block in each model the shear tests are performed and this time the curves are similar.

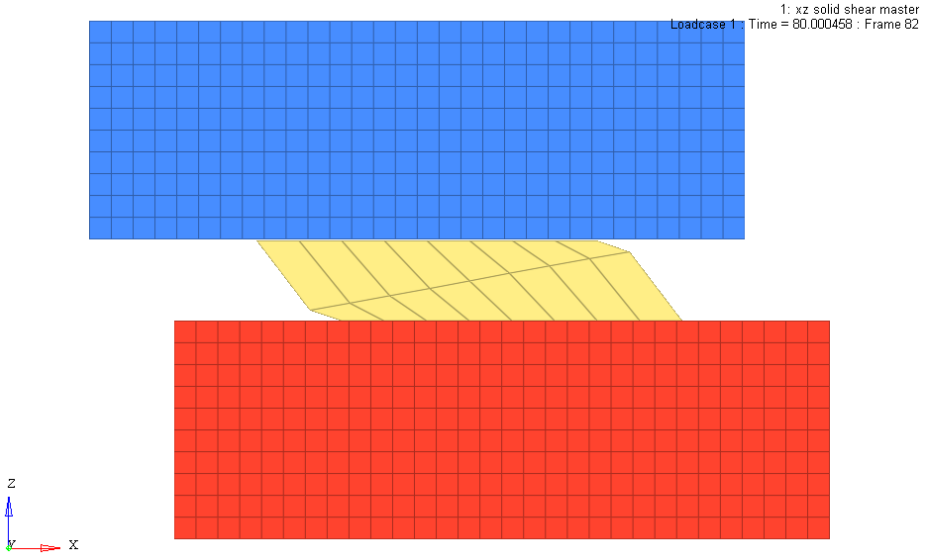


*Figure 32 Reduced height shear test*

In fact, usually shear tests are performed with specimen of reduced height but this showed that the hexahedral model is more affected by the geometric configuration compared to the shell model that retained the material behaviour also with different type of geometry.

Furthermore, an issue with the elastic stiffnesses was discovered. Indeed, extrapolating the elastic modulus from the compression tests, the value was much higher with respect to the ones obtained with the unit cell method. Comparing the models with shell and hexahedral for the same test, it is clear that the model with solid elements has a much more pronounced elastic region, so that the energy absorption characteristic of the plastic region could be hindered.

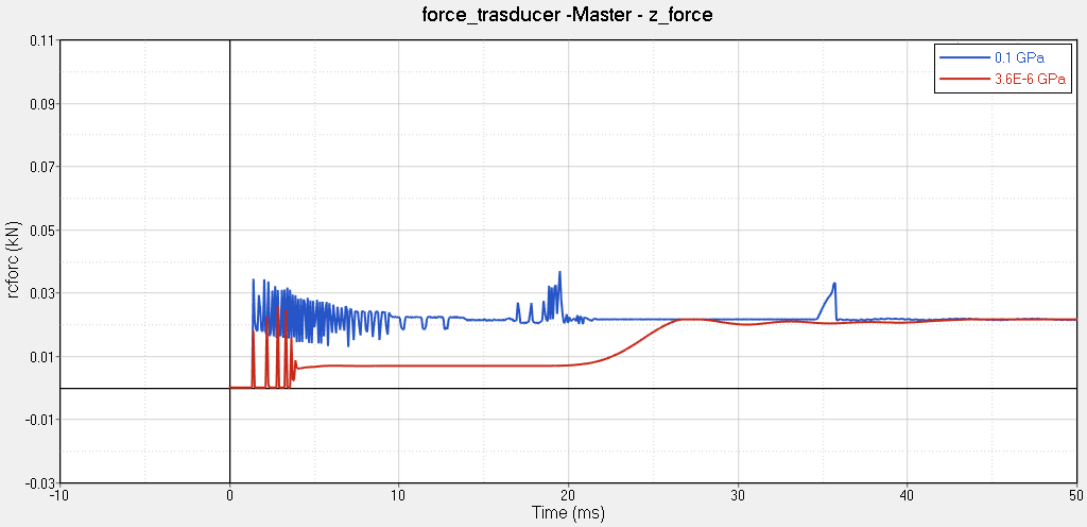


*Figure 33 solid compression comparison with different elastic moduli. Initial stage magnification*

In the figure the blue line is obtained with a higher elastic stiffness (0.1 GPa), more similar to the one obtained in the shell model, while the red one with the stiffness of the unit cell method (3.8 $10^{-6}$ GPa). The compression shown here is in X-axis and, although the energy not absorbed is negligible since the strong direction is Z, a bigger issue is linked to the elastic modulus. Summing up what already seen in MPDB optimization chapter, the material stress is updated computing a trail stress based on the interpolated stiffness, and comparing it to the stress value of the input curve, LCA in this case. If the trial stress is lower than the curve, the former will be used, otherwise the latter will. Since the interpolated stiffness is function of the uncompressed elastic modulus, the trial stress is therefore influenced and lower value are obtained and the stress values will not follow the input curve prescribed. This becomes visible in the simulations when the model with low elastic modulus is not able to follow the saturation behaviour of the honeycomb.

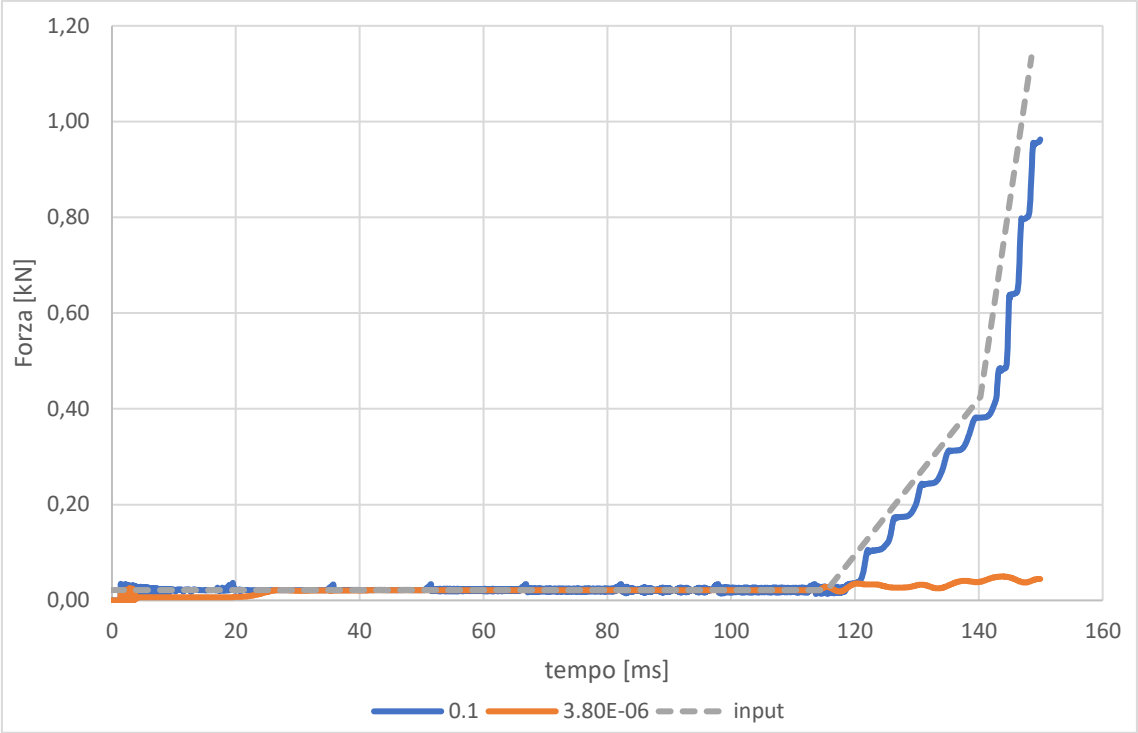


*Figure 34 solid compression comparison with different elastic moduli*

This issue led to the use of fictitious elastic moduli and so the results of the unit cell method were ignored from here on.

## 7.3 Tearing

The last honeycomb behaviour to be modelled is the tearing. All of the models seen in the review stage did not include the modelling of tearing, this because it is usually harder to do compared to shell-based model, where the entities are much smaller and deleting one of them to simulate a fracture does not influence much the stability of nearby elements and of the simulation itself. The tools explored to model tearing are the following or the combination of them:

- Tensile and Shear Strain at Failure fields in *MAT_MODIFIED_HONEYCOMB card
- *MAT_ADD_EROSION card
- *CONSTRAINED_TIED_NODES_FAILURE card
- Cohesive elements

The model used to test the different solutions is the same honeycomb block used for

compression tests, positioned on the plate from the same tests without any constraints. A number of different impactors have been used in order to have a tearing model as stable as possible. The main impactor used in the first phases is a cylinder shell, 200 mm tall and with a diameter of 60 mm, the thickness is 10 mm, which results in 3.17 kg of mass. The cylinder is launched head-on against the centre of the honeycomb block at a speed of 15 m/s (54km/h). Another configuration used in a successive phase is the same impactor, but rotate 90-degree along Z-axis, so that the lateral face of the cylinder hits the block first. Finally, another impactor shape is a prism, 200 mm tall and with 50 mm edge of the square base. The shell thickness is 10 mm so that the mass is 3.3 kg and the initial velocity is 20 m/s (72 km/h). Like before, the prism is positioned so that the lateral face hits the block first.

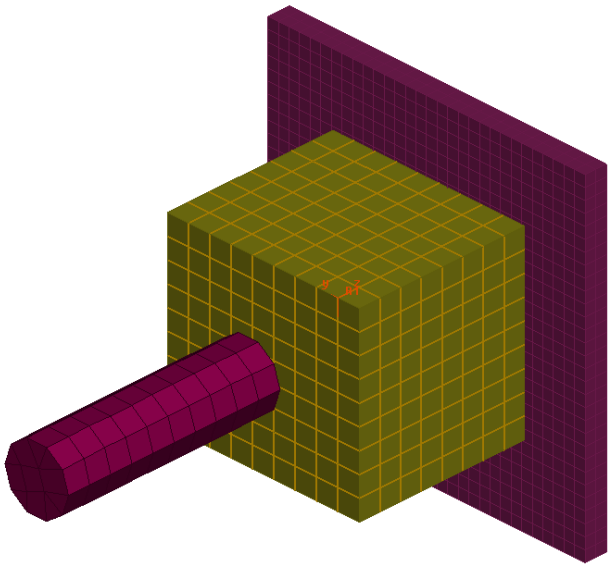

*Figure 35 Head-on cylinder for tearing modelling*

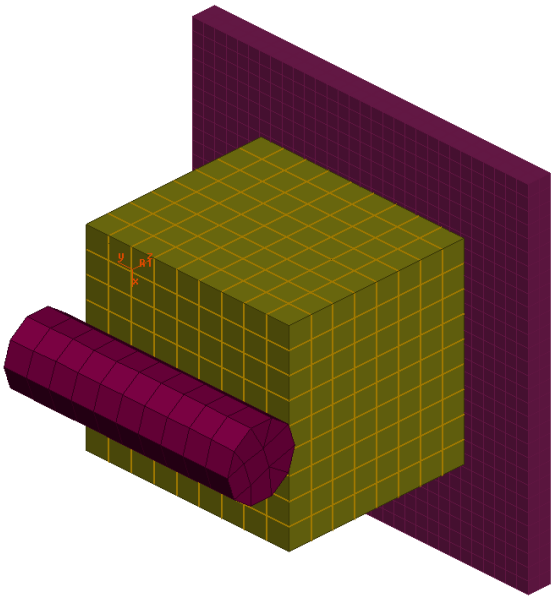

*Figure 36 Laid down cylinder for tearing modelling*

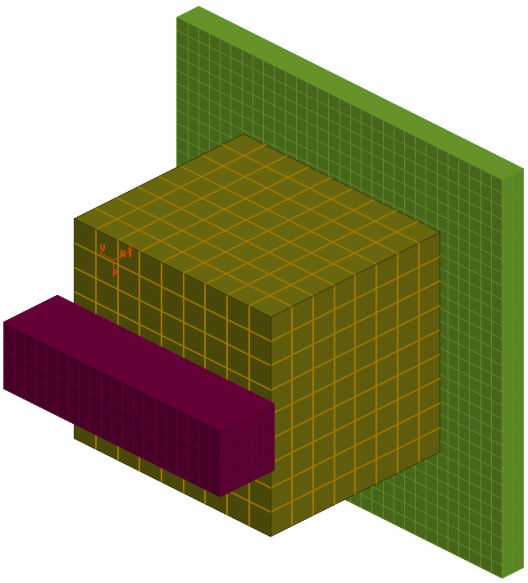

*Figure 37 Laid down prism for tearing modelling*

First of all, it was chosen to use a failure criterion because it was clear since the first simulations that the energy absorbed was overestimated. Indeed, with no failure criterion, the cells adjacent to the ones contacting directly the impactor would deform in shear and dissipate a large amount of energy. In this way the block behaves like a foam rather than like honeycomb. Unfortunately, it was not possible to conduct physical tests, but looking at similar tests in literature the impactor shape is very refined with clean separation of the honeycomb, determined by the tearing of the single wall surfaces and by the debonding of the double wall surfaces.

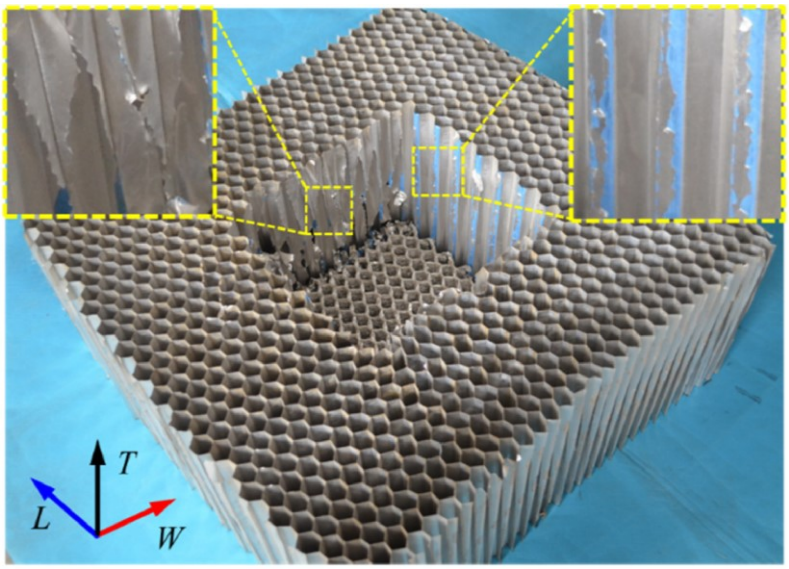


*Figure 38 Physical tearing test*

The first method tried was the Tensile and Shear Strain at Failure fields in *MAT_MODIFIED_HONEYCOMB card, but this soon was discarded if used alone. Although, during the first phase of testing, when using the head-on cylinder impactor, the block behaved fairly good. The elements heavily stressed around the impactor would erode (after having dissipated some energy) and a cleaner footprint in the honeycomb was obtained. At this point the laid-down cylinder configuration was tested. In this case the result was disappointing since the elements stressed in tensile or shear loads, that are going to be cancelled, are as big as a real honeycomb cell (400 $mm^2$) and the honeycomb block ended up split in three pieces.

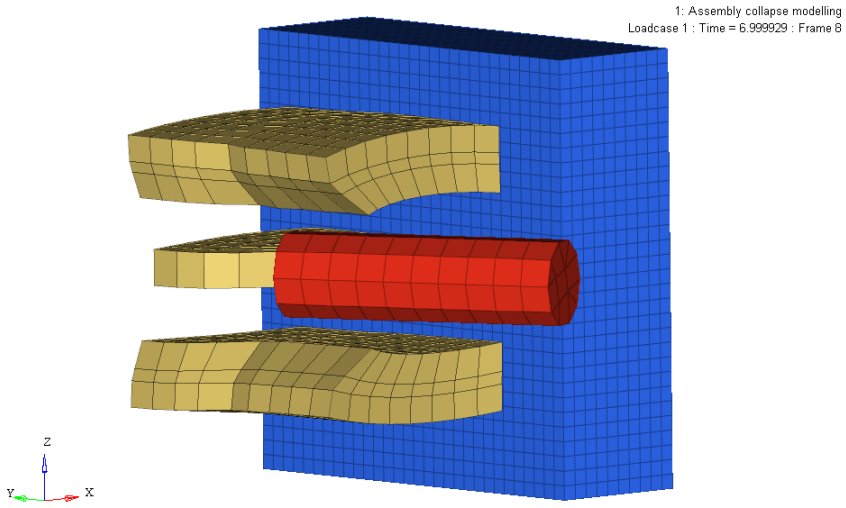


*Figure 39 TSEF-SSEF tearing modelling*

The card *MAT_ADD_EROSION provides a set of failure criteria to cancel elements, the main one for this case is VOLEPS, volumetric strain at failure. Although this card is useful to model the barrier bottoming-out and to avoid computational instabilities once the cells are fully compressed, it is not helpful for the tearing modelling. Furthermore, this card will not work with solid element formulation #0 and #9, not yet excluded at this stage of the tearing exploration.

The card *CONSTRAINED_TIED_NODES_FAILURE is the best candidate for this goal. It defines a tied node set with failure based on plastic strain (on volumetric for *MAT_MODIFIED_HONEYCOMB), and the nodes must be coincident. This means that a

node which normally would be shared between 8 hexahedral elements, in case of an internal node, have to be substituted by 8 nodes belonging to one and only one element but with the exact same coordinates.

So, in the pre-processor software, Ansa, the node release operation is easily done, but now the *SET_NODE have to be created. In order to work properly, one set has to be created containing only the nodes that shares the same coordinates and the constrain card is linked to this one set only. This leads to the creation of a huge number of sets, as many as the number of nodes originally belonging to the honeycomb block. So, the only reasonable way to proceed is creating a script via the tool present in Ansa, which interface a Python script to the model through dedicated functions. These functions are incredibly useful to collect data from the model, such as nodes, material, property information and are also able to write any data into the FEM model.

Obviously, these are only a small example of the potentialities baked in the script tool. Nonetheless, to write a functional and efficient Python script require a deep knowledge in coding, that is why I want to thank Engineer Alessandro Sias from FCA that kindly helps us writing the script.

Once the pre-processing phase is correctly finished, some problems started to appear. Even modifying the threshold value in the card for which the node should not be constrained anymore and should be set free to move independently, the card seemed to not work in the intended way. Indeed, when the threshold is equal to 0 all the nodes are rightly independent while when the threshold is greater than zero the nodes are constrained together throughout the entire simulation.

Having tried all the modifications and combinations, different tests were performed on an example model, so that the problem turned out to be the material when associated to the constrain card used. At this point we turn to Dynamore, the LS-Dyna technical support. Here I want to thank Engineer Pierre Glay for the insightful suggestions about the problems we were facing. Through the help of Dynamore developers, it was discovered that the card *CONSTRAINED_TIED_NODES_FAILURE does not work properly when combined with solid element formulation #0 and #9. So, using element formulation #1, the example model was able to model the tearing. It has to be specified

that the example model consists of a bullet hitting a plate, built with a single layer of solid elements. This involve that the elements are loaded in tensile stress and the nodes constrain will fail based on that. Another important suggestion that Eng. Glay gave was that using LS-PrePost as pre-processor, it is possible to automatically release the nodes and create the nodes sets and the constrain cards in few clicks.
When bringing back to the barrier model all this knowledge, it was not yet possible to model the tearing as well as initially expected. This is likely due to the different kind of solicitation with respect to the example model. While in the example all the elements are loaded in tensile stress, in the barrier model a high concentration of compressive stress is present, leading to think that this may have compromised the card logic and to abandon this solution for the model.

Finally, having going through the LS-Dyna manual multiple times in search for a solution, the cohesive elements were chosen. These elements are placed between every hexahedral element surface in contact with another element. And by controlling the failure of these elements it is possible to let the hexahedral elements move independently after a certain threshold is reached. The element formulation is #19, peculiar for solid cohesive elements, while the material used *MAT_COHESIVE_ELASTIC. This material is very simple but provides differential stiffness and failure values for axial and tangential loads, that is just what is needed. To include these elements into the model LS-PrePost comes in handy again because it includes an element generation tool capable of automating the creation process, unlike Ansa. An important point to highlight is the time step influence. Although the cohesive elements are solid and the volume is close to zero, they do not influence the timestep like regular solid elements. Fearing that cohesive could influence the results obtained before, a compression test is performed to check if any different behaviour is detected and luckily no dissimilarities were observed.
The first test performed for tearing was the one with the prismatic impactor, so that sharp edges help discovering if this solution is any good. Indeed, if it does not manage to work in this condition where the cohesive elements are directly stresses heavily, it is

difficult to imagine performing better in tougher situations.

Once the right threshold is found the barrier was able to model correctly the failure criterion. Below the comparison images between the model with cohesive (on the right) and without (on the left) follows. The model without cohesive elements is the baseline and does not have any failure criteria.

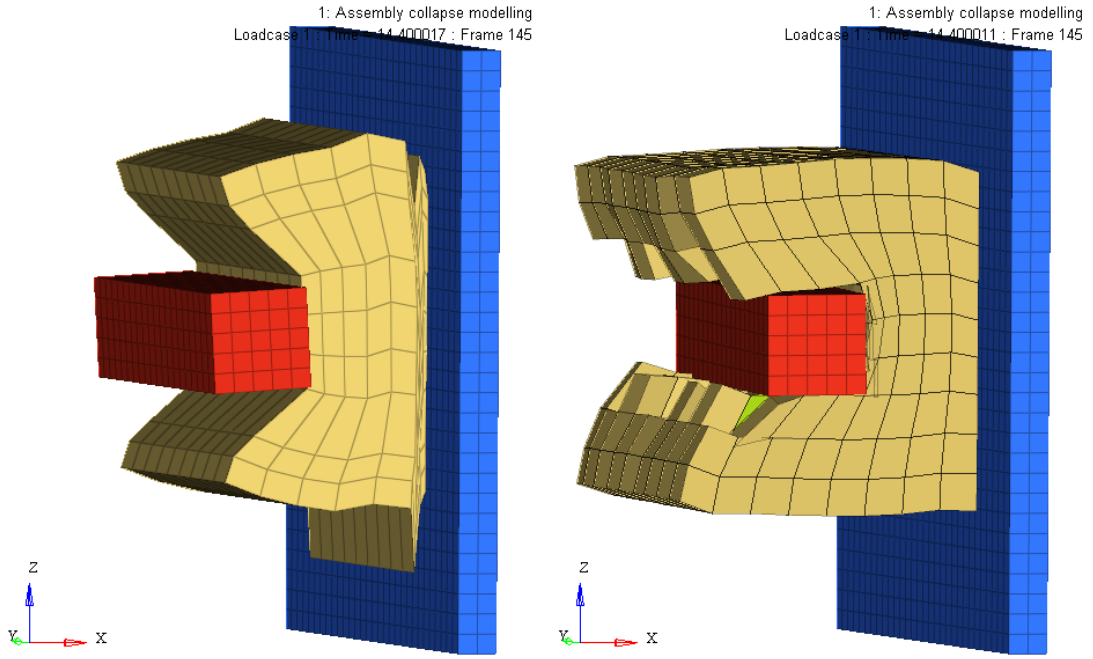


*Figure 40 cohesive elements laid-down prism impactor tearing test*

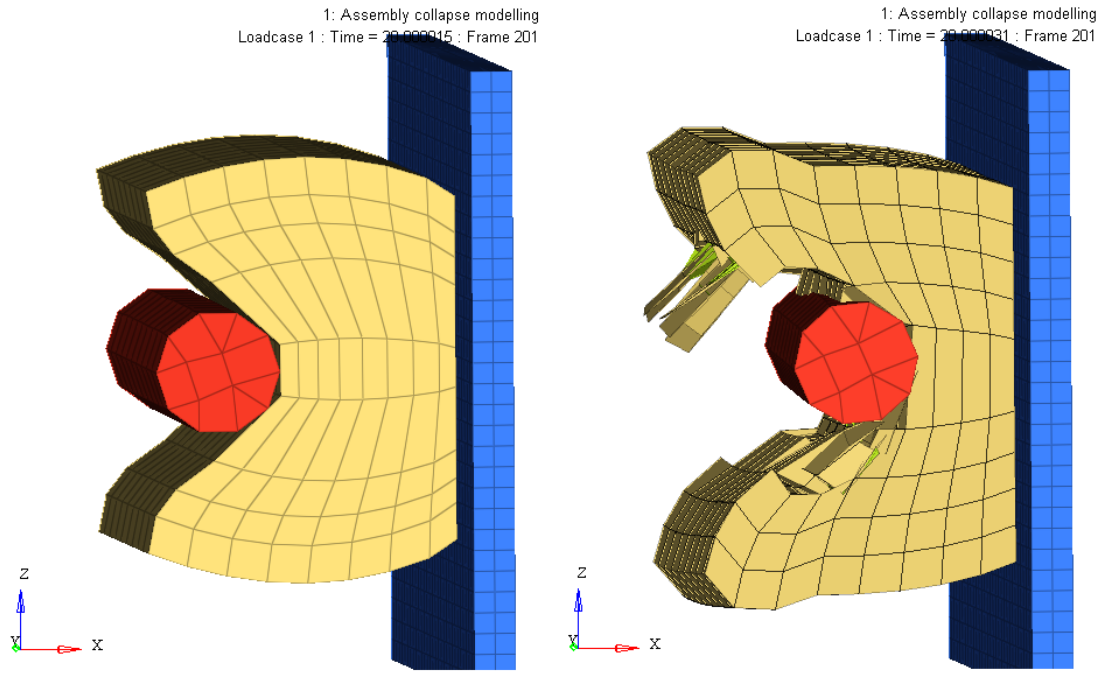


*Figure 41 cohesive elements laid-down cylinder impactor tearing test*

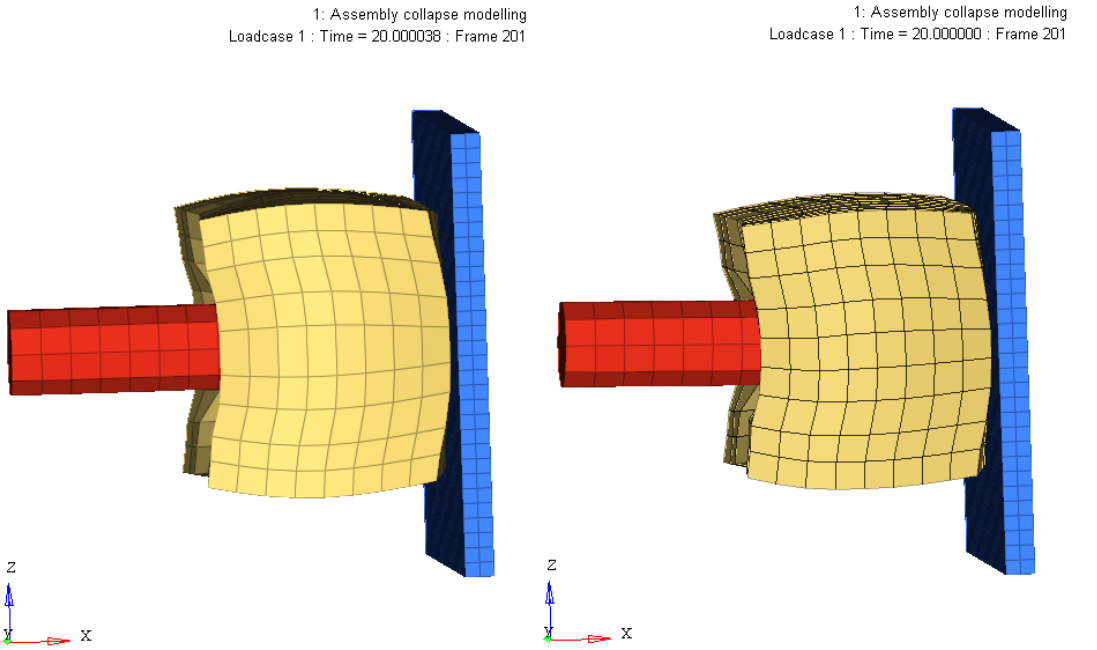


*Figure 42 cohesive elements head-on cylinder impactor tearing test*

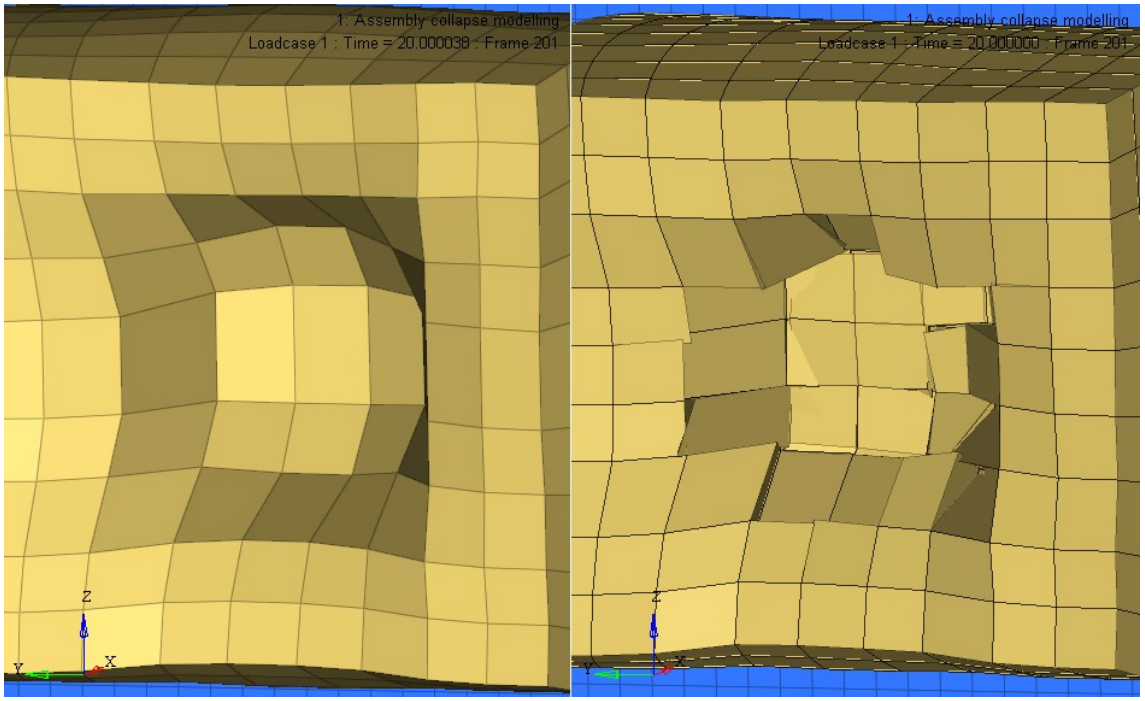


*Figure 43 cohesive elements head-on cylinder impactor tearing test (impactor not shown)*

It is important to note that the results are obtained only with cohesive elements, with no contribution of others failure criteria. As it will be explained later, in the full-scale barrier test a combination of cohesive elements, *MAT_ADD_EROSION and Tensile and Shear Strain at Failure is used and it will provide positive results, even better than these

just shown. Moreover, two different calibration of cohesive failure criteria will be used, one more resistant than the other, keeping in mind the manufacturing characteristics of honeycomb blocks.

# 8. Material characterization in full scale model

Now that the honeycomb block is fully characterized in scale form, the full front block is taken into consideration. Initially to confirm what has been done, a compression test is performed to check if the same results are obtained, and so it was.

The test performed to calibrate more accurately the failure criteria was the Euro NCAP barrier homologation test, but only including the front block. Repeating what said in a previous chapter, the test consists in a rigid tubular frame mounted on a trolley, travelling at 60 km/h and weighting 1300 kg. The force output computed as reacting force of the rigid wall placed behind the honeycomb block, has to be inside the crash corridor prescribed. Since only the first block is used, just the first portion of corridor is considered, up to 200 mm of barrier deflection.

In the initial stages the force output and so the energy absorbed was extremely low. With the main cause being the contact used. Indeed, in the simulations it was possible to see that the block's cell, after a certain deformation, would penetrate the impactor and would not deform, leading to the reduced energy absorption.

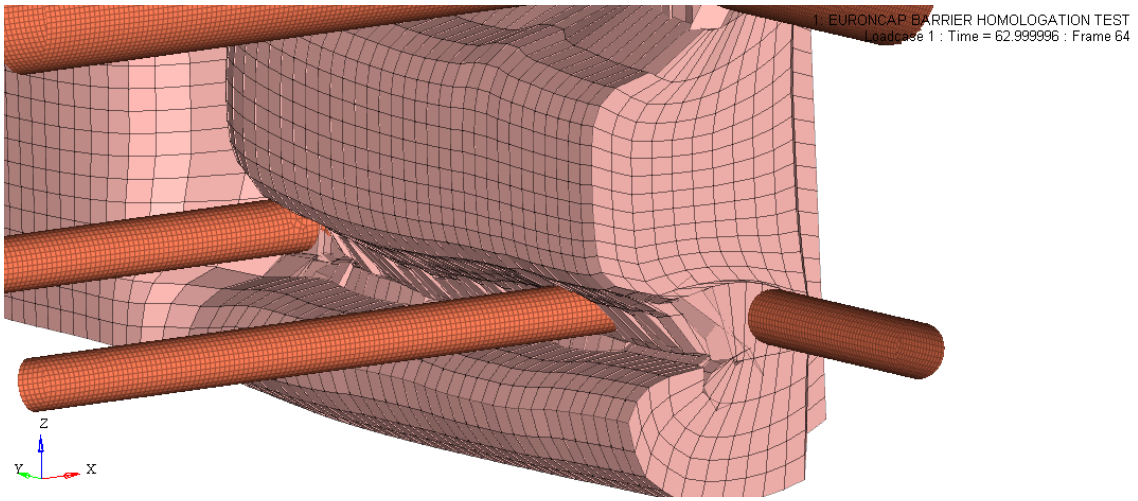


*Figure 44 Full front block contact penetration #1*

The behaviour shown in the figure above could be explained by the use of a single surface contact, like the one initially used, *CONTACT_AUTOMATIC_SINGLE_SURFACE. As a matter of facts, this type of contact considers all the parts as slave, so only the nodes take part to the contact algorithm. This issue can be solved in different ways, like using a one-way contact (putting the block as the master part) or a two-way contact. These

contacts have the peculiarity to take into account the segments that connect the node in the master side (for one-way) or in both sides (for two-ways). Indeed, if the segment is not considered, could happen that a node would penetrate a slave surface without reacting with any force, as shown in this slide from LSTC.

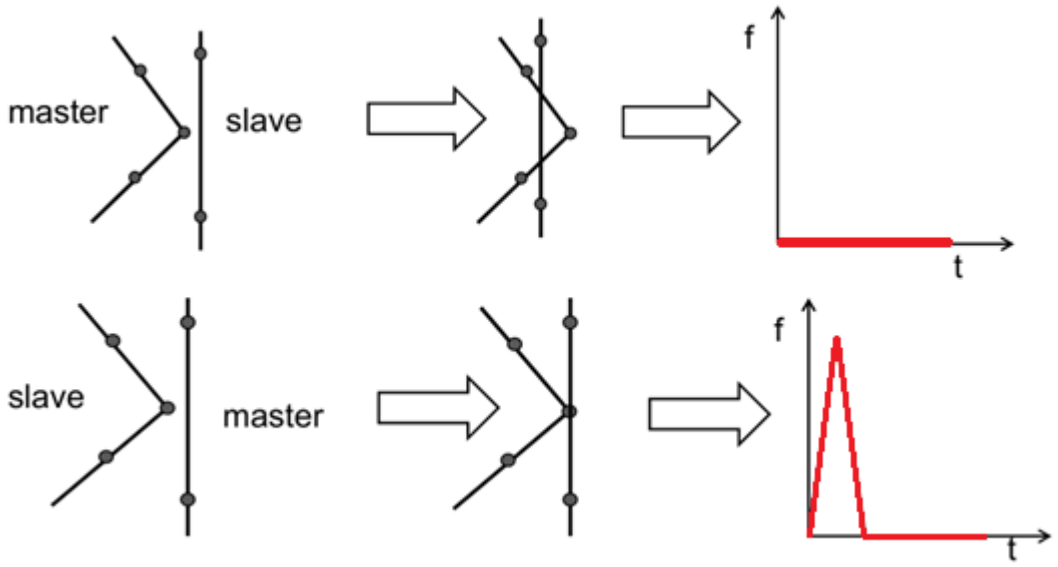


*Figure 45 Master-Slave contact forces*

A similar result can be obtained forcing the segment-based algorithm into the single surface contact, via the option SOFT=2, which will be better explained later.

Another solution could be to use a finer mesh in the block so that the nodes are closer to each other and the penetration is less likely. But this would affect very negatively the simulation time and so it is not tested.

A final alternative, the one eventually applied, is the use of a more robust contact, like *CONTACT_AUTOMATIC_GENERAL. This contact is similar to a single surface but it has the peculiarity to store three possible segments for each node instead of two like the single surface does.

When this solution was applied unfortunately the penetration was still obvious in large regions of the model. In the figure below the impactor has been partially hidden so that the penetration would be visible.

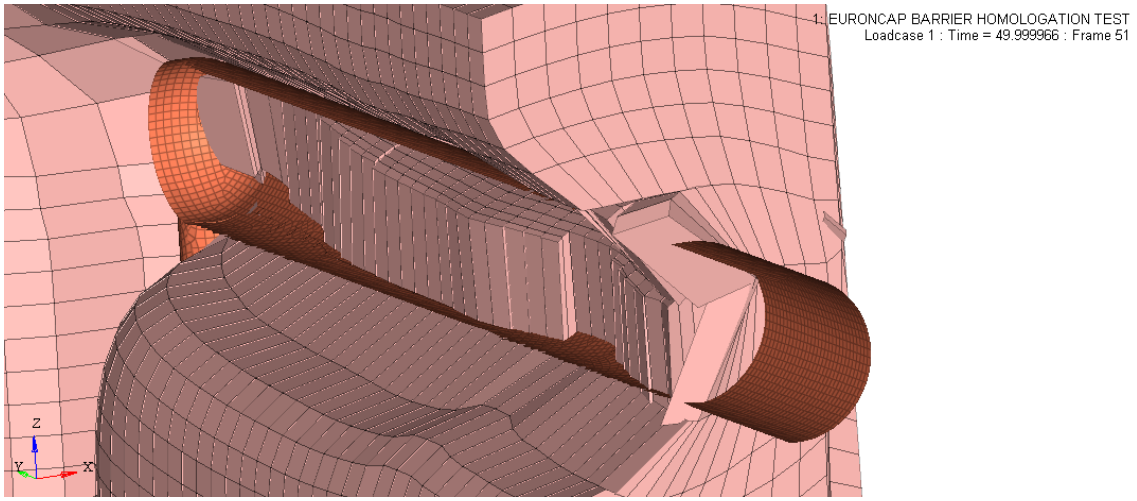


*Figure 46 Full front block contact penetration #2*

After some investigation it was discovered that some elements in contact with the impactor would erode after a substantial deformation, leaving the elements behind facing the rigid body. But since the second row of elements is not considered in the contact algorithm, the block would no longer sense the contact from the impactor in those areas. To solve this issue the *CONTACT_ERODING_SINGLE_SURFACE is used. The eroding kind of contact will update the contact surface every time an element included in the contact set is deleted due to material failure criteria. The contact used is based on the previously employed *CONTACT_AUTOMATIC_SINGLE_SURFACE, so the option SOFT=2 for contact-based contact is enabled.

The contact in this way worked properly but obviously a simulation time deficit was inevitable. As a try the segment-based contact option was disabled to recover some time and the contact kept working properly, leading to think that the problem encountered before was not caused by nodes-to-nodes contact instead of segments-to-segments, but rather by the cancellation of the first row of elements.

To improve things further, after many iterations looking for the right threshold for the cohesive elements, the elements did not deform so massively in z-direction because the cohesive between hexahedrals would fail and so the likely of nodes penetration is slimmer if it was ever going to be a problem.

Concerning cohesive elements, a simple gimmick was used to model better the tearing of the honeycomb. All the cohesive elements were assigned to two different material law, one stronger than the other. The stronger one was the one perpendicular to x-axis,

the one supposed to keep in together the columns of honeycomb cell when are being compressed. This is compliant with physical test where failure of the cells along global x-axis is possible due to the compression load applied to them. Instead all the other cohesive elements, perpendicular to y and z axes, have a calibrated failure in order to model the tearing and debonding characteristic of the honeycomb.

Following all these considerations the block model started to behave as expected, at least in the first part of the simulation.

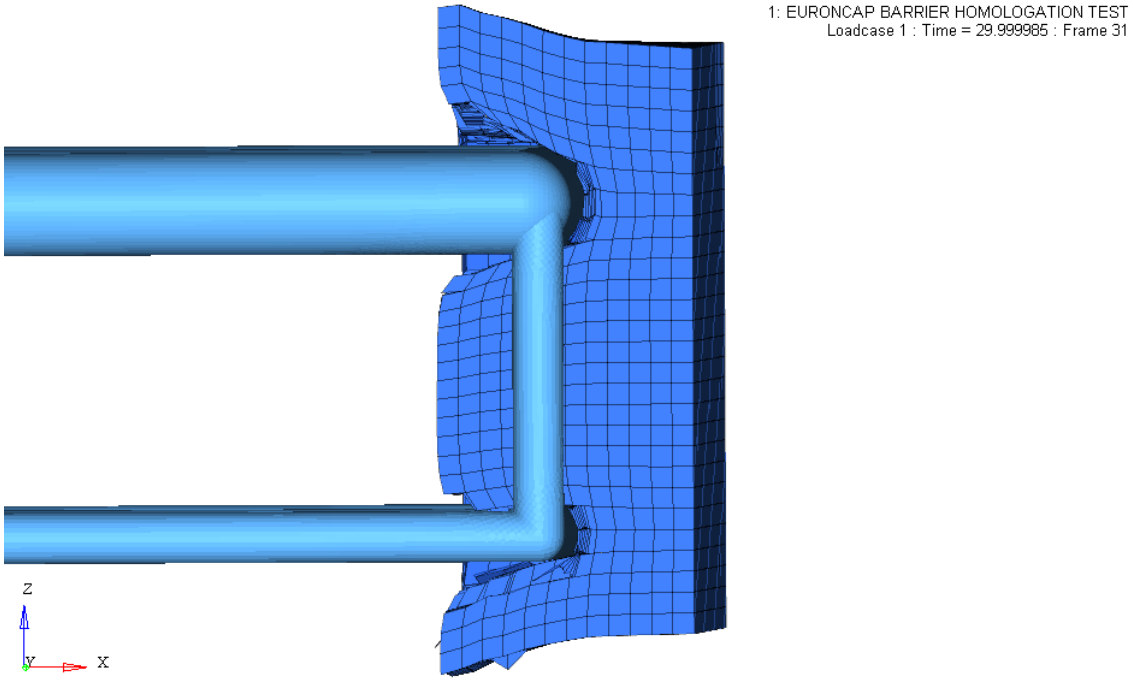


*Figure 47 Front block impactor test*

It is important to note that this behaviour has been obtained by scaling up the shear curve for the material card. That was necessary because, as explained in the previous chapter, the shear resistance of the material is much lower than the real one in tall models. This caused the cells to distort much easily, leading to compression instabilities or a shear deformation so high that the elements would be deleted due to negative volume. Instead by scaling by a factor of 10 the shear input curves (LCAB, LCBC, LCCA), the cells are more stable and behave correctly.

However, in this simulation, like in all the others done before, the model would run into instability issues. This is expected because the block is fully compacted against a rigid wall and so the nodes would lose the contact and would be shot all over the place. But

it is noted that some instability is caused by cells extremely deformed in shear, like in the figure below.

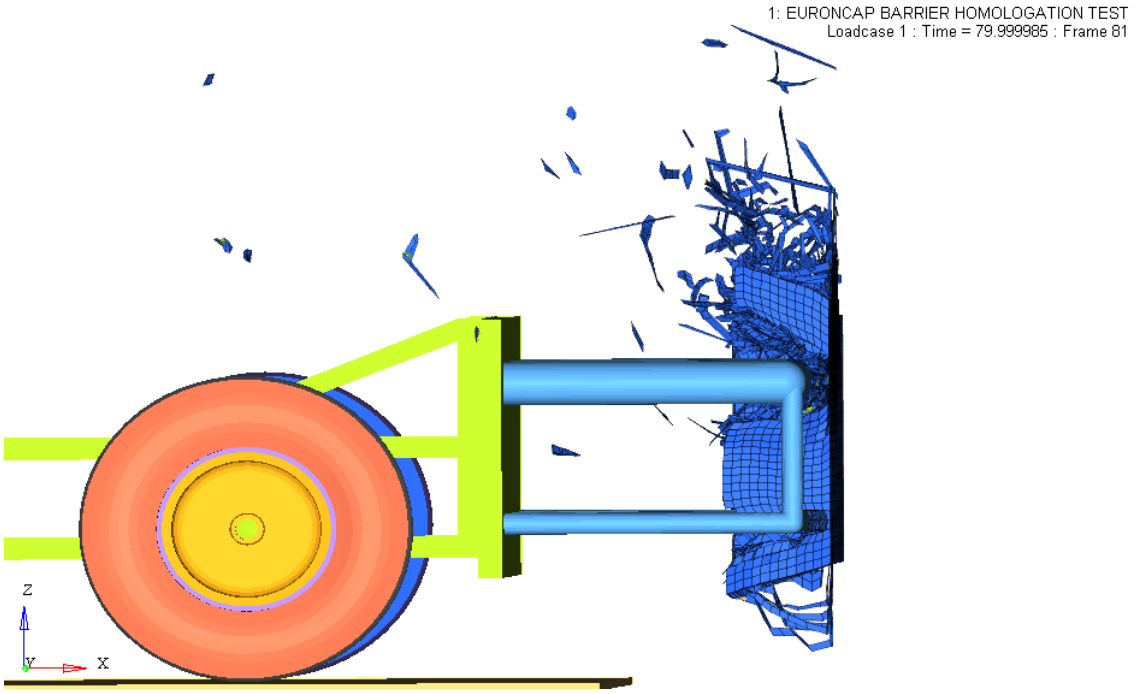


*Figure 48 Front block impactor test - numerical instability*

To solve these stability issues two countermeasures are taken. The first one is a failure criterion in shear, the aforementioned SSEF field in the material card, with a really high threshold (1.6) in order to delete only the elements that are severely distorted, that could cause instabilities, and not the ones near the impactor that are being correctly deformed. The other criterion is a relative volume threshold, present in the VOLEPS field in the *MAT_ADD_ERODION card. This criterion provides a twofold improvement since it avoids instabilities when the cells are so compressed that the nodes would lose the contact but also helps to model the bottoming out of the block. Indeed, when the cells are completely compressed, they cannot absorb any more energy and so it is good practise to delete them to avoid computation instabilities and to let the trolley (or vehicle) impacts against the wall behind the block or the full barrier.

After ensuring that the honeycomb was behaving as wanted, the next step is to check if the force curve would wall inside the prescribed crash corridor. But unfortunately, the result was way off what expected.

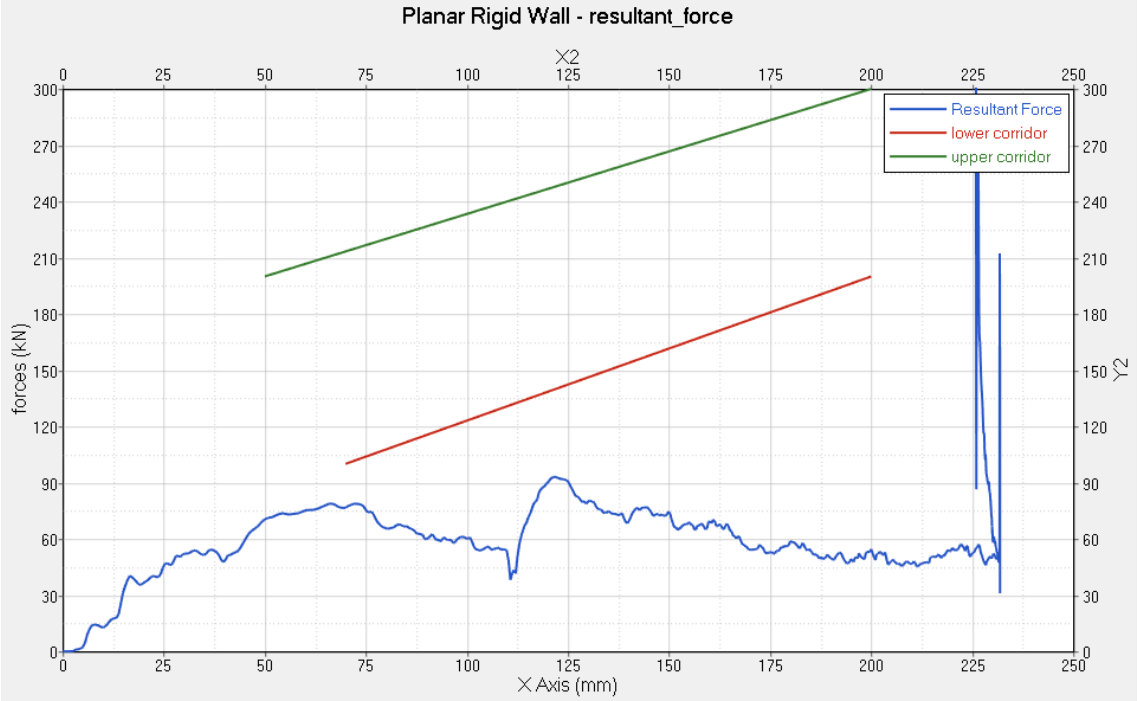


*Figure 49 Front block impactor test – resultant force graph*

In the figure only the first part of the crash corridor is shown since only the front block has been tested for the time being. So, to investigate better the issue the front block from the shell model built by LSTC is tested and it yields similar results. Instead, when testing the block together with the front contact sheet, the resulting force fell inside the crash corridor, up to a deformation of 165 mm.

So, the outer skin is added to the hexahedral model as well. But differently from the shell model, the contact plate is modelled as a thin shell and not a thick one. Instead, just like in the reference model, the material used is *MAT_PIECEWISE_LINEAR_PLASTICITY and the glue is modelled with beam elements with element formulation #9, spotweld beam, and material *MAT_SPOTWELD. The peculiarity of the glue is that each beam is connected to the contact plate and to a node of the hexahedral element. As a matter of facts, since the cells do not share any nodes between each other, the nodes with same coordinates, facing the outer skin, are four, instead of just one. For this reason, a beam has to be connected to each node in order to avoid stress concentration and uneven adhesive bonding.

The simulations including the contact plate provided an increased force output, leading to the fact that a much larger portion of the block is interested by the impact. Indeed,

the central portion of the block between the tubular impactor is compressed thanks to the outer plate and the portion of the block on the left of the impactor is bent inward due to the action of the glue.

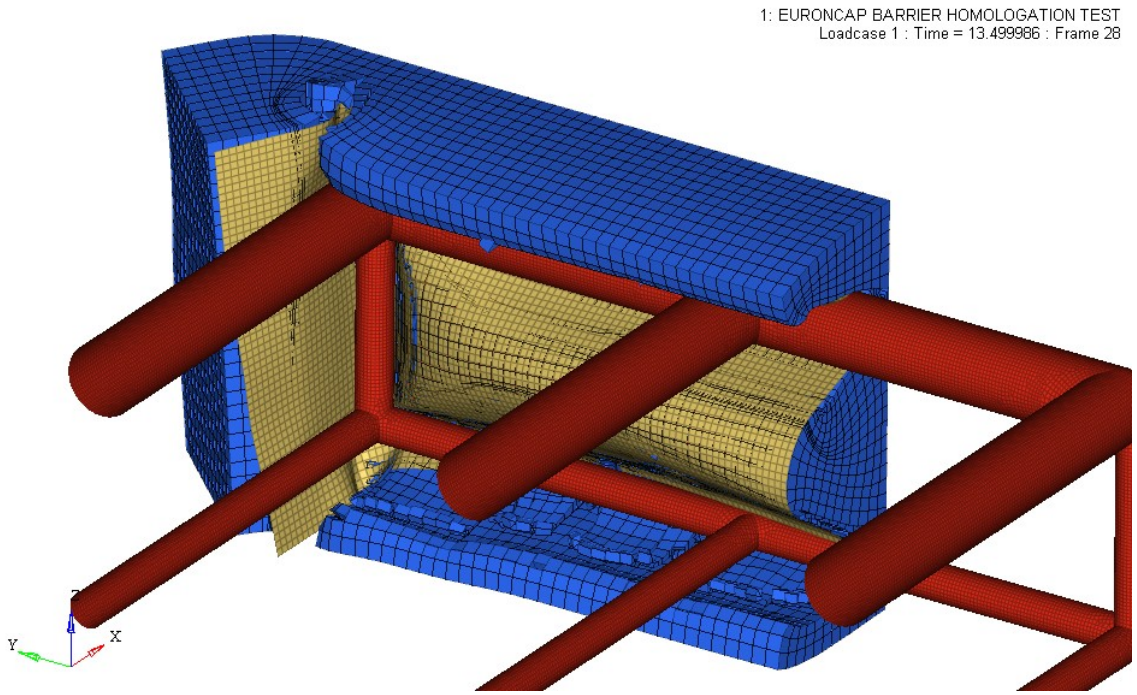


*Figure 50 Contact plate influence in front block impactor test*

But even after having calibrated again the failure thresholds for cohesive, glue and outer skin, the force would be inside the corridor only for a small interval of barrier deflection, dropping soon after. However, it was noted that if the cohesive threshold were calibrated to high value so that no fail would occur, the resultant force would fit inside the corridor. But since the goal of this thesis is a more representative model of the barrier, this option was discarded.

A final attempt changing the mesh size is done. Up to now the elements had the dimension of the actual cell in the front block, 19.1 mm, so it was decided to change this value to 40 mm. Following this modification much better results started to appear, likely caused by the fact that a larger quantity of mass is distributed per each node, improving the stability under compression. This is due to the very high sensitivity of the model to mass variation, linked to the extremely low density, in the $10^{-8}$ order of magnitude.

The curve is inside the corridor for an extensive amount of barrier deflection, but the coarser mesh in the block would create some problems with the nearby and finer

contact plate. Indeed, the nodes of the block would penetrate the outer skin between nodes and from that point on the contact algorithm would lock those two portions together leading to a kind of bonding, as shown below. This problem would drag down some portion of the block that in normal circumstances would stay in place.

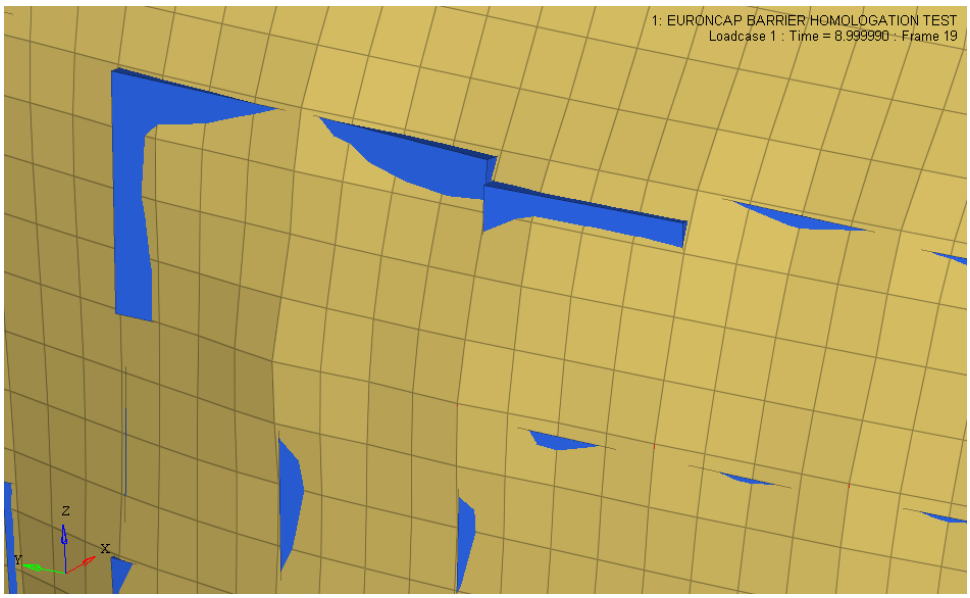


*Figure 51 Element penetration with coarser mesh*

To solve this and to avoid using a computational-heavy global contact algorithm, a *CONTACT_AUTOMATIC_NODES_TO_SURFACE is used. This is a one-way contact with a master part, the skin, and a slave node set, the first row of nodes of the block. This contact avoids that the master segments between each pair of nodes is penetrated by any slave nodes and, since it is heavier than a single surface contact, it is localized only to the region needing this modification.

Great improvements were obtained also in the simulation time. On the same server of 32 core provided by the project HPC PoliTO, the simulation with mesh size of 19 mm lasted just shy of 4 hours, while with mesh size of 40 mm the time reduced to 50 minutes. This is explained obviously by the fact that less hexahedral elements are present, but with that also an extremely reduced number of cohesive elements are present and the eroding contact would refresh less frequently the contact surface, since the element in the set are less and more stable. To put the termination time into context, for the shell model the run was completed in a 28 cores server provided by FCA in 27 minutes. Even if the two server CPUs have different cores-count, the overall performance are the same,

making these termination times comparable.

The shell model, however, has a suboptimal failure modelling. Indeed, the honeycomb block tends to wrap around the tubular impactor and this behaviour is due to two causes. First of all, the honeycomb failure is not aggressive enough and so the cells would not separate, while the second cause is a too much resistant glue that keeps block and contact plate connected for too long, according to the physical tests seen.

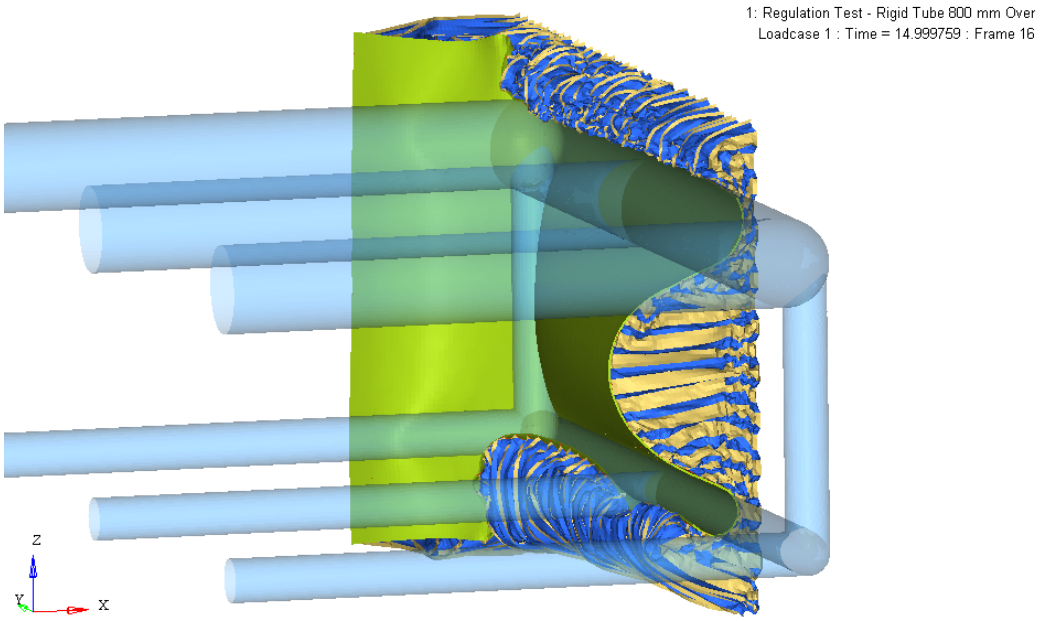


*Figure 52 Shell model front block impactor test*

Finally, the curves obtained from the models are shown.

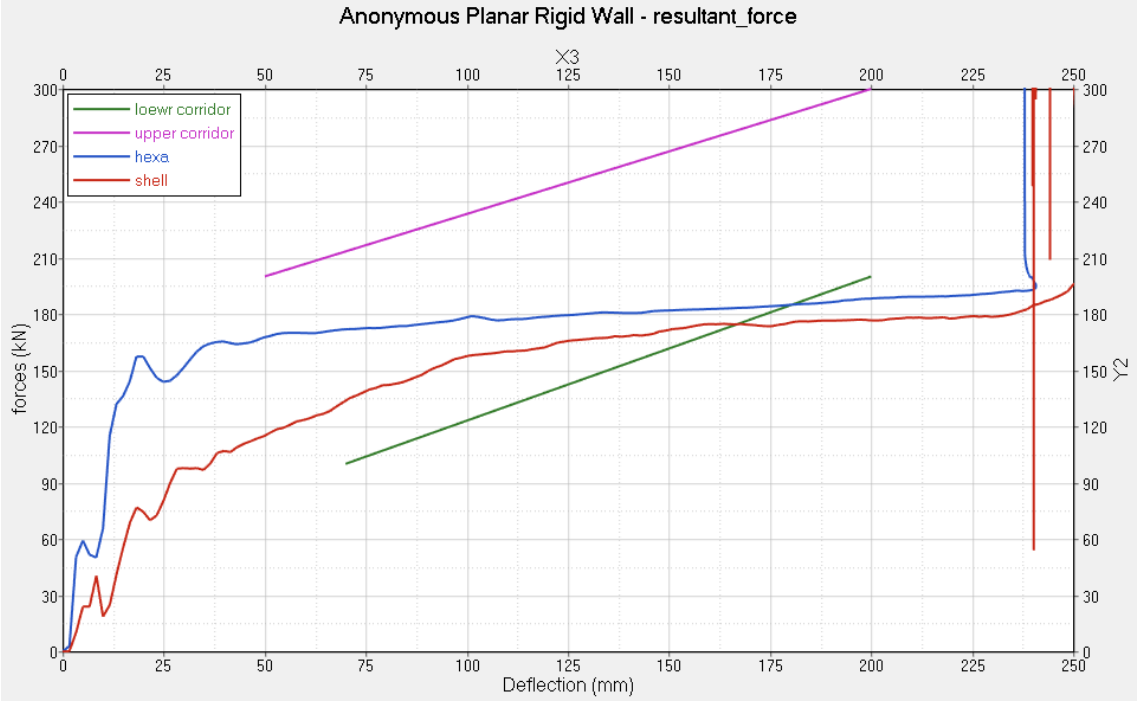


*Figure 53 Hexahedral and shell models forces in impactor test*

# 9. Results from entire barrier

Now that the front block is fully characterized, the next step is to test the full barrier with all three blocks and relative intermediate sheets and glue. Unfortunately, due to lack of time caused by all the problems encountered and by the pandemic situation that precluded any work not done by remote that could have speed things up, this full barrier model is quickly built without all the attentions deserved to the front block.

The middle and rear blocks are built similarly to the front one, with hexahedral elements measuring 40 mm each edge. The middle block is 450 mm deep and the rear block just 90 mm, while the other two common measures are 1000 mm length and 570 mm height. These blocks have also cohesive elements in order to model the failure with different thresholds for each block, since the force levels are different. In the honeycomb material card, the density is changed since the difference in resistance comes from a denser cells' arrangement. The input curves for compression and shear resistance are scaled up by a factor equal to the ratio between crash strengths prescribed in the Euro NCAP technical bulletin. So, considering the rear block, the ratio is equal to 5 since the maximum prescribed crash strength is 1.711 MPa for the rear block and 0.342 MPa for the front block. A similar approach is used with the middle block but, since the resistance is not constant, it is good practice to split the part into slices and assign to each of them an increasing level of constant strength. The middle block has been divided into 5 slices and the graph below shows the strength corridor prescribed by Euro NCAP for this block and in grey the different levels of crash resistance of the different slices. These values are respectively 0.750, 0.828, 0.906, 0.983 and 1.061 MPa and according to them also the other input curves are scaled. Moreover, since each slice has different strength, a different cohesive material is assigned with threshold increasing as resistance does.

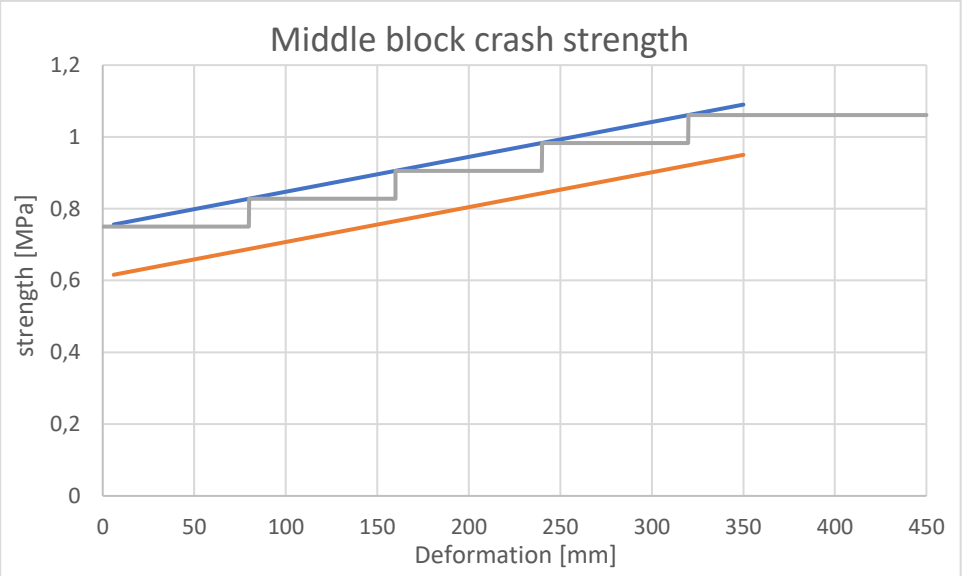


*Figure 54 Middle block strength levels*

The glue holding together the blocks and the sheets are modelled, just like before, as spotweld beam with calibrated failure. The intermediate plates are built starting from the contact plate already available changing the thickness, 0.5 mm in this case, and the effective strain at failure in the material card.

The cladding and the rear plate are reused from LSTC model, just like the bonding method to connect contact plate and cladding and rear block and back plate. Indeed, a *CONTACT_TIED_NODES_TO_SURFACE is used, imposing as slave the contact plate nodes facing the cladding and the glue nodes behind the rear block that face the rear plate. All the other contacts already used with the front block are ported over, modifying the set of the involved parts. Below the full barrier model discussed is shown.

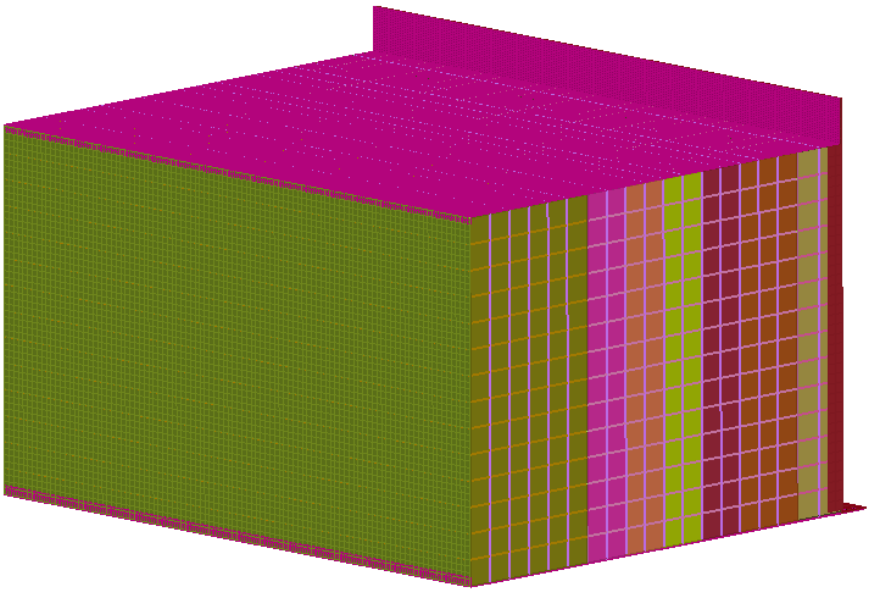

*Figure 55 Full MPDB virtual model*

After some iterations, the right failure thresholds are found for cohesive elements and the resulting force and deformed barrier are as follow.

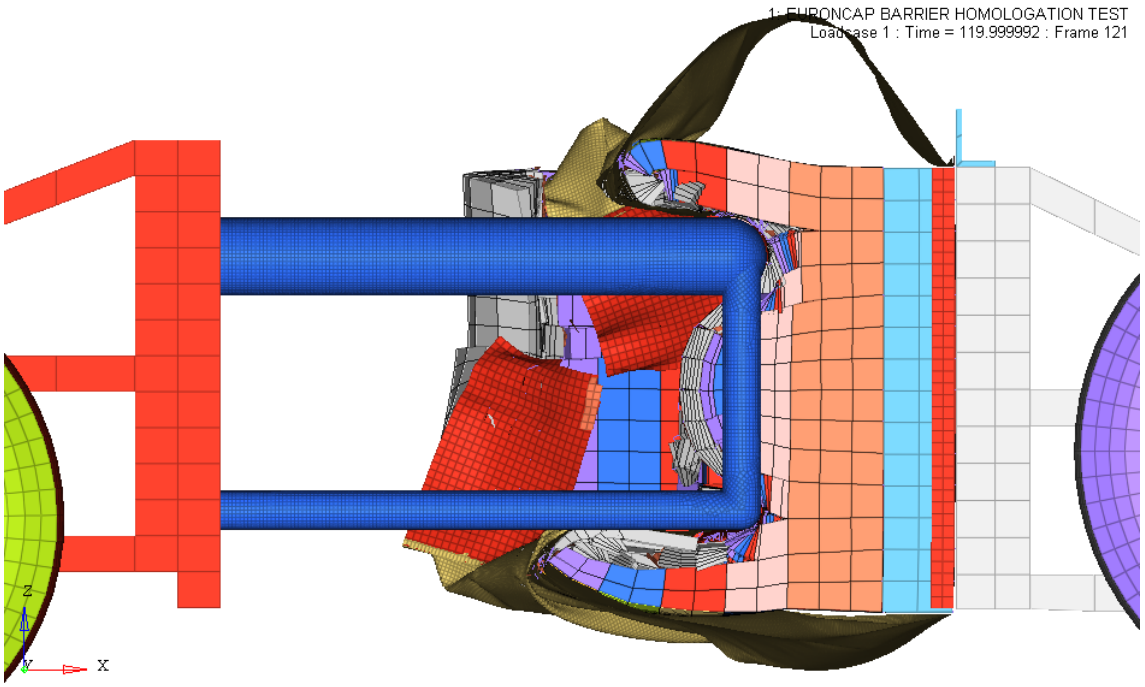


*Figure 56 Euro NCAP barrier homologation test*

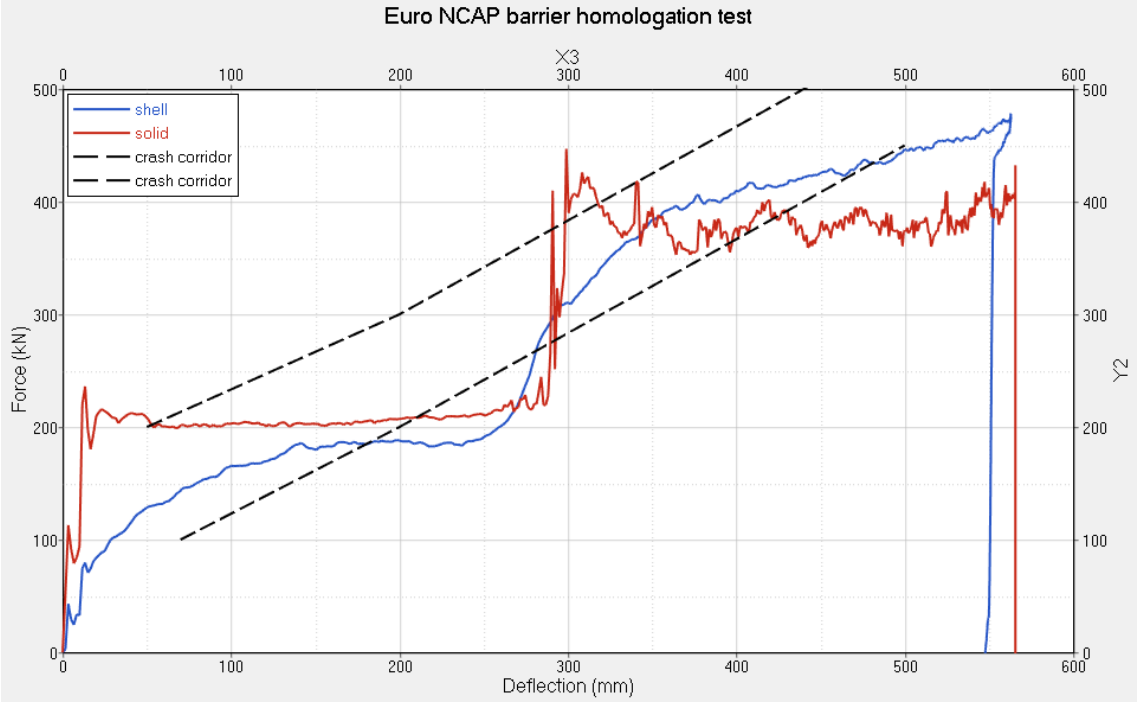


Finally, a virtual frontal crash test is performed, following the procedure prescribed by Euro NCAP for MPDB testing. The goal is to test both the reference barrier model by LSTC and the barrier designed in this thesis, since a better failure criterion should lead to more realistic results. The vehicle used has been provided by FCA and both the trolley which the barrier is mounted on and the vehicle travel at a speed of 50 km/h towards each other. The alignment is done so that the outer edge of the barrier hits the vehicle exactly in the middle, resulting in a 50% overlap. The trolley with barrier has a mass of 1400 kg, while the car, complying with Euro NCAP regulations, will account also the mass of four occupants and their luggage.

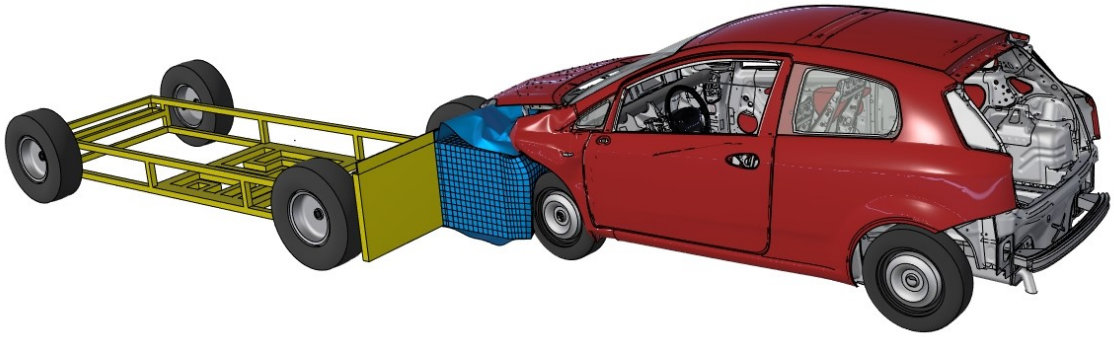

*Figure 57 Vehicle to barrier crash test*

When comparing the solid and shell barriers for the same Moving Progressive Deformable Barrier test, a similar behaviour is highlighted, with a better penetration of

the vehicle crash structures for the model developed in this thesis. Indeed, a vehicle in early stage of development is chosen so that highly localized forces are experienced.

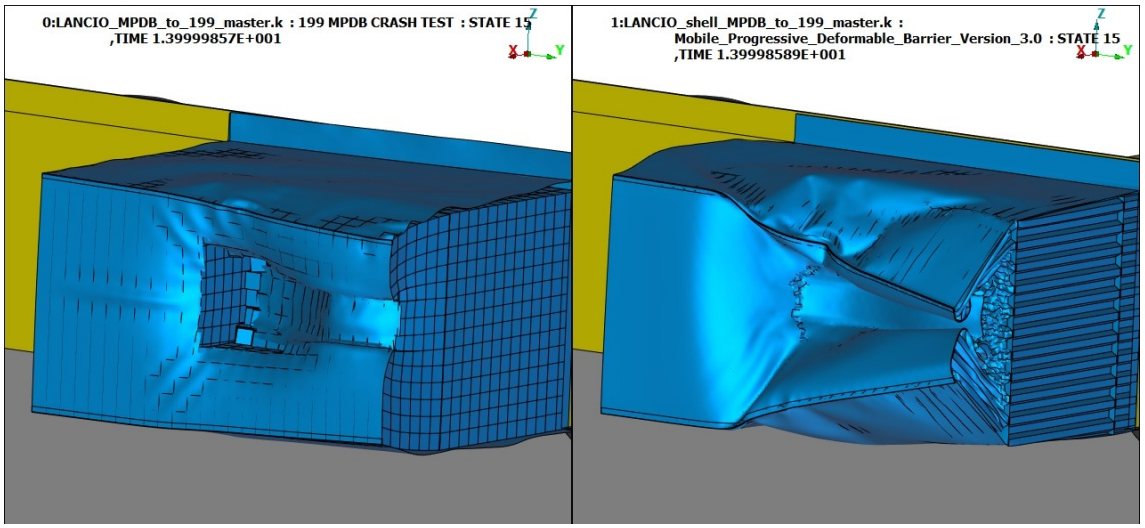


*Figure 58 Solid and shell barriers crash test comparison*

Looking at the vehicle deceleration curves the two barriers produce similar deceleration profiles and same peak values. Both models are able to model the bottoming of the barrier. This happens when the vehicle goes through the entire barrier and hits the rigid plate behind it, so that the highest deceleration value is to be expected.

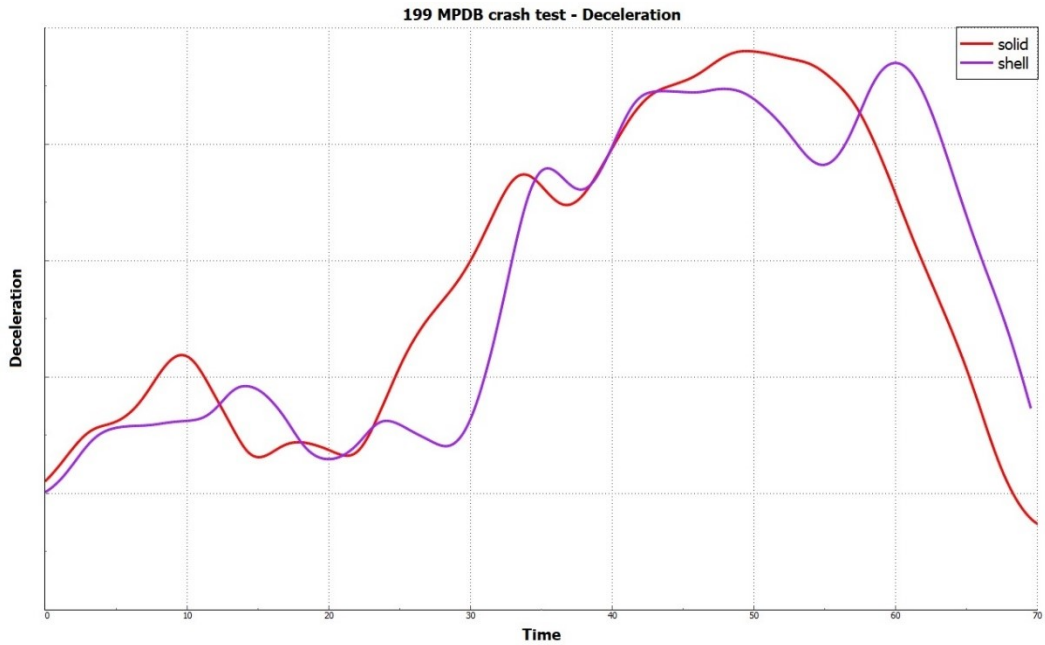


*Figure 59 Vehicle deceleration in MPDB crash test*

Finally, in these tests a remarkable reduction in simulation time is noticed, from 48 hours for the shell model, to 29 hours for the solid one.

# 10.

# 10. Conclusion

This thesis dealt with a finite element model for a frontal crash barrier. The different steps include the honeycomb material characterization through scaled and full-scale tests and finally the entire barrier is considered and a virtual crash test is performed with a vehicle supplied by FCA.

When looking at the entire work it is possible to say that the solutions adopted for the barrier model proved to be very effective in their intent. The use of hexahedral elements and *MAT_MODIFIED_HONEYCOMB is consistent with the alternatives to shell models, while a distinctive characteristic of this barrier is its failure criteria and its ability of modelling the bottoming of the barrier.

In the characterization phase of the honeycomb blocks some problems have been faced, leading to discover that for this application accurate modelling of the elastic range can be detrimental for the overall behaviour of the honeycomb. Another finding is that the material chosen would not behave ideally when a tall specimen is subjected to shear loads. Afterwards, different alternatives have been examined in order to obtain an accurate failure criterion and most of them proved to be not satisfactory. Finally, the failure has been modelled using cohesive elements with calibrated failure thresholds.

In the simulations with the entire barrier, different contact algorithms have been evaluated since some problem with penetrations have been experienced.

Then dynamic tests with a trolley and with a vehicle have been performed and the failure criterion chosen proved to be a major advantage of this barrier model, due to its ability of modelling in a better way tearing and debonding of the honeycomb when compared to the reference barrier, and performing just as good with the bottoming of the barrier.

A further improvement to this model could be the optimization of the simulation time, through the variation of the mesh size and of the material parameters so that the timestep can be increased without compromising the barrier's behaviour.

## APPENDIX - Summary of cards used, with values

In this chapter all the cards peculiar to this model are included and to avoid any repetitions, only the ones for the front block are considered.

*CONTROL_TERMINATION

| endtim | endcyc | dtmin | endeng | endmas | nosol |
|---|---|---|---|---|---|
| 20 | 0 | 0.1 | 0 | 3 | 0 |

*CONTROL_TIMESTEP

| dtinit | tssfac | isdo | tslimt | dt2ms | lctm | erode | ms1st |
|---|---|---|---|---|---|---|---|
| 0 | 0.9 | 0 | 0 | -2.00E-05 | 0 | 1 | 0 |
| dt2msf | dt2mslc | imscl | unused | unused | rmscl | unused | ihdo |
| 0 | 0 | 0 | 0 | 0 | | | |

*CONTACT_ERODING_SINGLE_SURFACE_ID

| cid | title | | | | | | |
|---|---|---|---|---|---|---|---|
| 1Global_Self_Contact | | | | | | | |
| ssid | msid | sstyp | mstyp | sboxid | mboxid | spr | mpr |
| 6 | 0 | 2 | 0 | 0 | 0 | 0 | 0 |
| fs | fd | dc | vc | vdc | penchk | bt | dt |
| 0.3 | 0.2 | 0 | 0 | 0 | 0 | 0 | 1.00E+20 |
| sfs | sfm | sst | mst | sfst | sfmt | fsf | vsf |
| 1 | 1 | 0.8 | 0 | 1 | 1 | 1 | 1 |
| isym | erosop | iadj | | | | | |
| 0 | 0 | 0 | | | | | |
| soft | sofscl | lcidab | maxpar | sbopt | depth | bsort | frcfrq |
| 0 | 0.1 | 0 | 1.025 | 2 | 2 | 0 | 1 |
| penmax | thkopt | shlthk | snlog | isym | i2d3d | sldthk | sldstf |
| 0 | 0 | 0 | 0 | 0 | 0 | 0 | 0 |
| igap | ignore | dprfac | dtstif | unused | unused | flangl | cid_rcf |
| 1 | 1 | 0 | 0 | 0 | 0 | | |

*CONTACT_AUTOMATIC_NODES_TO_SURFACE_ID

| cid | title | | | | | | |
|---|---|---|---|---|---|---|---|
| 3pelle_to_blocco_1way_contact | | | | | | | |
| ssid | msid | sstyp | mstyp | sboxid | mboxid | spr | mpr |
| 4 | 6 | 4 | 3 | 0 | 0 | 0 | 0 |
| fs | fd | dc | vc | vdc | penchk | bt | dt |
| 0.3 | 0.2 | 0 | 0 | 0 | 0 | 0.0 | 1.00E20 |
| sfs | sfm | sst | mst | sfst | sfmt | fsf | vsf |
| 1 | 1 | 0.8 | 0 | 1 | 1 | 1 | 1 |
| soft | sofscl | lcidab | maxpar | sbopt | depth | bsort | frcfrq |
| 0 | 0.1 | 0 | 1.025 | 2 | 2 | 0 | 1 |
| penmax | thkopt | shlthk | snlog | isym | i2d3d | sldthk | sldstf |
| 0 | 0 | 0 | 0 | 0 | 0 | 0 | 0 |
| igap | ignore | dprfac | dtstif | unused | unused | flangl | cid_rcf |

| | | | | | | | |
|---|---|---|---|---|---|---|---|
| 1 | 1 | 0 | 0 | 0 | 0 | | |
| *PART | | | | | | | |
| title | | | | | | | |
| colla | | | | | | | |
| pid | secid | mid | eosid | hgid | grav | adpopt | tmid |
| 5 | 5 | 5 | 0 | 0 | 0 | 0 | 0 |
| *SECTION_BEAM_TITLE | | | | | | | |
| colla | | | | | | | |
| secid | elform | shrf | qr/irid | cst | scoor | nsm | naupd |
| 5 | 9 | 1 | 2 | 1 | 0 | 0 | 0 |
| ts1 | ts2 | tt1 | tt2 | print | | | |
| 1 | 1 | 0 | 0 | 0 | | | |
| *MAT_SPOTWELD_TITLE | | | | | | | |
| colla | | | | | | | |
| mid | ro | e | pr | sigy | eh | dt | tfail |
| 5 | 1.00E-06 | 2 | 0.3 | 0.202 | 0.02 | 0 | 0 |
| efail | nrr | nrs | nrt | mrr | mss | mtt | nf |
| 0 | 0.20 | 0.15 | 0.15 | 0 | 0 | 0 | 30 |
| *PART | | | | | | | |
| title | | | | | | | |
| pelle | | | | | | | |
| pid | secid | mid | eosid | hgid | grav | adpopt | tmid |
| 6 | 6 | 6 | 0 | 0 | 0 | 0 | 0 |
| *SECTION_SHELL_TITLE | | | | | | | |
| pelle | | | | | | | |
| secid | elform | shrf | nip | propt | qr/irid | icomp | setyp |
| 6 | 16 | 0 | 0 | 1 | 0 | 0 | 1 |
| t1 | t2 | t3 | t4 | nloc | marea | idof | edgset |
| 2.3 | 2.3 | 2.3 | 2.3 | 0 | 0 | 0 | 0 |
| *MAT_PIECEWISE_LINEAR_PLASTICITY_MIDFAIL_TITLE | | | | | | | |
| pelle | | | | | | | |
| mid | ro | e | pr | sigy | etan | fail | tdel |
| 6.27E-05 | 70 | 0.3 | 0.1 | 0 | 0.2 | 0 | |
| c | p | lcss | lcsr | vp | | | |
| 0 | 0 | 3 | 0 | 0 | | | |
| eps1 | eps2 | eps3 | eps4 | eps5 | eps6 | eps7 | eps8 |
| 0 | 0 | 0 | 0 | 0 | 0 | 0 | 0 |
| es1 | es2 | es3 | es4 | es5 | es6 | es7 | es8 |
| 0 | 0 | 0 | 0 | 0 | 0 | 0 | 0 |
| *PART | | | | | | | |
| title | | | | | | | |
| blocco | | | | | | | |
| pid | secid | mid | eosid | hgid | grav | adpopt | tmid |
| 7 | 7 | 7 | 0 | 0 | 0 | 0 | 0 |

*SECTION_SOLID_TITLE
blocco

| secid | elform | aet |
|---|---|---|
| 7 | 1 | 0 |

*MAT_MODIFIED_HONEYCOMB_TITLE
blocco

| mid | ro | e | pr | sigy | vf | mu | bulk |
|---|---|---|---|---|---|---|---|
| 7 | 1.53E-08 | 500 | 0.49 | 0.1 | 0.1 | 1.00E-10 | 0 |
| lca | lcb | lcc | lcs | lcab | lcbc | lcca | lcsr |
| 921 | 920 | 922 | 0 | 918 | 917 | 919 | 0 |
| eaau | ebbu | eccu | gabu | gbcu | gcau | aopt | macf |
| 0.1 | 0.1 | 0.1 | 0.1 | 0.1 | 0.1 | -1 | 1 |
| xp | yp | zp | a1 | a2 | a3 | | |
| 0 | 0 | 0 | 0 | 0 | 0 | | |
| d1 | d2 | d3 | tsef | ssef | vref | tref | shdflg |
| 0 | 0 | 0 | 0 | 1.6 | 0 | 0 | 0 |

*PART
title
cohesive

| pid | secid | mid | eosid | hgid | grav | adpopt | tmid |
|---|---|---|---|---|---|---|---|
| 8 | 8 | 8 | 0 | 0 | 0 | 0 | 0 |

*SECTION_SOLID_TITLE
cohesive

| secid | elform | aet |
|---|---|---|
| 8 | 19 | 0 |

*MAT_COHESIVE_ELASTIC_TITLE
cohesive

| mid | ro | roflg | intfail | et | en | fn_fail | ft_fail |
|---|---|---|---|---|---|---|---|
| 8 | 1.50E-06 | 0 | 3 | 1 | 10 | 10 | 0.004 |

*PART
title
cohesive_strong

| pid | secid | mid | eosid | hgid | grav | adpopt | tmid |
|---|---|---|---|---|---|---|---|
| 9 | 9 | 9 | 0 | 0 | 0 | 0 | 0 |

*SECTION_SOLID_TITLE
cohesive_strong

| secid | elform | aet |
|---|---|---|
| 9 | 19 | 0 |

*MAT_COHESIVE_ELASTIC_TITLE
cohesive_strong

| mid | ro | roflg | intfail | et | en | fn_fail | ft_fail |
|---|---|---|---|---|---|---|---|
| 9 | 1.50E-06 | 0 | 3 | 100 | 100 | 10 | 10 |

*MAT_ADD_EROSION_TITLE
Default_MAT_ADD_EROSION

| mid | excl | mxpres | mneps | effeps | voleps | numfip | ncs |
|---|---|---|---|---|---|---|---|
| 7 | 0 | 0 | 0 | 0 | 0.95 | 1 | 1 |
| mnpres | sigp1 | sigvm | mxeps | epssh | sigth | impulse | failtm |
| 0 | 0 | 0 | 0 | 0 | 0 | 0 | 0 |

*DEFINE_COORDINATE_NODES_TITLE
local_coordinates_material

| cid | n1 | n2 | n3 | flag | dir |
|---|---|---|---|---|---|
| 1 | 313 | 314 | 976 | 0X | |

# Acknowledgements

To conclude I want to take some moments to thank all the people that made this thesis possible. Thanks to professor Alessandro Scattina for the constant support and availability shown. Thanks to engineer Erik Baldoin for the endless hours dedicated to me to make this thesis possible. Thanks to all the personnel from FCA and CRF I came in touch with during my internship period that helped me to realize this thesis.

Thanks to the company that let me use its informatic infostructures, like the computational cluster and the personal workstation accessed remotely.

Additionally, thanks to the project hpc@polito for the computational resources provided http://hpc.polito.it

Finally, thanks to my family and to my friends for supporting me in the entire study duration away from home and for being an outlet when needed.

# Reference


Brian Wlker, I. B. (2006). A New Generation of Crash Barrier Models for LS-DYNA. *LS-DYNA Anwenderforum, Crash II(Verbindungstechnik)*. Ulm.

Ellway, J. (2018, November). Euro NCAP MPDB Specification. *Version 1.2*.

Euro NCAP. (2013, July). Assessment Protocol - Adult Occupant Protection. *Version 6.0*.

Euro NCAP. (2018, November). MPDB frontal impact testing protocol. *Version 1.0*.

Euro NCAP. (n.d.). *Euro NCAP*. Retrieved 10 27, 2020, from www.euroncap.com

*Finite Element Method*. (n.d.). Retrieved from Wikipedia: https://en.wikipedia.org/wiki/Finite_element_method

L. Morello, L. R. (2011). *The Automotive Body* (Vol. Volume II: System Design). Springer.

Livermore Software Technology Corporation. (2013, January 30). LS-DYNA keyword user's manual. *Volume I, Revision 2645*.

Livermore Software Technology Corporation. (2013, January 30). LS-DYNA keyword user's manual. *Volume II(Material Models), Revision 2645*.

Lorna J. Gibson, M. F. (1999). *Cellular Solids: Structure ans Properties.* Cambridge University Press.

LSTC. (n.d.). *Products: LS-Dyna*. Retrieved from LSTC: https://www.lstc.com/products/ls-dyna

Penado, F. E. (2013, October). Effective elastic properties of honeycomb core with fiber-reinforced composite cells. *Open journal of composite materials, Vol 3(No. 4)*. Scientific Research.

Shanqing Xu, J. H. (2012, July). Experimental study of the out-of-plane dynamic compression of hexagonal honeycombs. *Composite Structures*. Elsevier.

Shubham V. Rupani, S. S. (2017, April). Design, Modelling and Manufacturing aspects of Honeycomb Sandwich Structures: A Review. *Volume 2(Issue 4)*. International Journal of Scientific Development and Research.

Thomas Jost, T. h. (2008). A new method to model aluminium honeycomb based crash barrier in lateral and frontal crash load cases. *LS-DYNA Anwenderforum, Crash III(Barrieren), Versagen*.

Yuanjie Liu, W. Z. (2020, January). Testing and modelling tearing and air effect of aluminium honeycomb under out-of-plane impact loading. *International journal of impact engineering, Vol 135*. Elsevier.